# NEURO-WAVELET BASED ISLANDING DETECTION TECNHIQUE

A THESIS IN ELECTRICAL ENGIEERING

*Master of Science in Electrical Engineering*

Presented to the faculty of the American University of Sharjah
College of Engineering
in partial fulfillment of
the requirements for the degree

MASTER OF SCIENCE

By

YARA FAYYAD
B.S. 2008

Sharjah, UAE
May 2010

We approve the thesis of Yara Fayyad

Date of signature

_____ _____

Dr. Ahmed Osman
Assistant Professor, Electrical Engineering, AUS
Thesis Advisor

_____ _____

Dr. Ayman El Hag
Assistant Professor, Electrical Engineering, AUS
Graduate Committee

_____ _____

Dr. Ehab El-Saadany
Visiting Associate Professor, Electrical Engineering
Petroleum Institute, Abu Dhabi, UAE
Graduate Committee

_____ _____

Dr. Mohamed El-Tarhuni
Associate Professor, & Department Head
Coordinator, Electrical Engineering Graduate Program

_____ _____

Dr. Hany El-Kadi
Associate Dean, College of Engineering

_____ _____

Dr. Yousef Al Assaf
Dean, College of Engineering

_____ _____

Mr. Kevin Lewis Mitchell
Director, Graduate & Undergraduate Programs & Research

NEURO-WAVELET BASED ISLANDING DETECTION TECHNIQUE

Yara Fayyad, Candidate for the Master of Science Degree

American University of Sharjah, 2010

# ABSTRACT

Integrating distributed generator into the existing distribution network is predicted to play an important role in the near future. Distributed generators, specifically renewable energy technologies, such as photovoltaic, wind-turbine and fuel cells are entering a stage of fast expansion. The Electric Power Research Institute estimates that distributed generations account for 20% of all new generations going online in the US.

Connecting distributed generator to the distribution network has many benefits such as increasing the capacity of the grid and enhancing the power quality. However, it gives rise to many problems. This is mainly due to the fact that distribution networks are designed without any generation units at that level. Hence, integrating distributed generators into the existing distribution network is not problem-free. Unintentional islanding is one of the encountered problems. Islanding is the situation where the distribution system containing both distributed generator and loads is separated from the main grid as a result of many reasons such as electrical faults and

their subsequent switching incidents, equipment failure, or pre-planned switching events like maintenance.

In this thesis a passive Neuro-wavelet based islanding detection technique has been developed. The proposed method utilizes and combines wavelet analysis and artificial neural network to detect islanding. The technique is based on the transient voltage signals generated during the islanding event. Discrete wavelet transform is capable of decomposing the signals into different frequency bands. It can be utilized in extracting discriminative features from the acquired voltage signals. The features are then fed to a trained artificial neural network model which is if well trained capable of differentiating between islanding event and any other transient events such as switching or temporary fault. The trained classifier was then tested using novel voltage waveforms. The test results indicated that this approach can detect islanding events with high degree of accuracy.

# CONTENTS:

# LIST OF FIGURES:

# LIST OF TABLES:

# LIST OF ABBREVIATIONS:

| | | |
|---|---|---|
| AFD | - | Active frequency drift |
| ANN | - | Artificial Neural Network |
| CB | - | Circuit breaker |
| CWT | - | Continuous wavelet transform |
| db | - | a particular mother wavelet – daubechies mother wavelet |
| DG | - | Distributed generators |
| DH | - | Detection of harmonics |
| DWT | - | Discrete Wavelet Transform |
| FFT | - | Fast Fourier transform |
| IEEE | - | Institute of Electrical and Electronics Engineers |
| LLG | - | Line to line to ground fault |
| NDZ | - | Non detective zones |
| P | - | Active power |
| PCC | - | Point of common coupling |
| PF | - | Power Factor |
| PJD | - | Phase jump detection |
| PLCC | - | Power line carrier communication |
| PLL | - | Phase Locked Loop |
| PV | - | Photovoltaic panel |
| Q | - | Reactive Power |
| $Q_f$ | - | Quality factor |
| ROCOF | - | Rate of change of frequency |
| RLC | - | resistive, inductive and capacitive (as in RLC load) |

| | | |
|---|---|---|
| RMS | - | root mean square |
| SFS | - | Sandia frequency shift |
| SLG | - | Single line to ground fault |
| SMS | - | Slip mode frequency shift |
| STFT | - | short time Fourier transform |
| SVM | - | space vector modulation |
| THD | - | Total harmonic distortion |
| UOF | - | Under/Over frequency |
| UOV | - | Under/Over voltage |

# ACKNOWLEDGMENT

In the name of *Allah*, most Gracious, most Merciful.

First of all, all praise and glory be to *Allah*, the Almighty, for enlightening my way and directing me to accomplish this small objective successfully.

I would like to express my sincere gratitude and deep appreciation to my supervisor, Dr. Ahmed Osman, for the invaluable guidance, patience, encouragement, and valuable countless hours of attention he dedicated throughout this work. He provided me with important suggestions, significant ideas, and helpful materials to develop this thesis. May *Allah* reward him in this world and the Hereafter.

I am also grateful to my graduate committee: Dr. Ayman El Hag and Dr. Ehab El Saadany for their effort, discussions and constructive comments.

Special thanks go to all faculty members of the department of Electrical Engineering in the American University of Sharjah for their valuable advice and guidance.

I will always be thankful to my friends and colleagues for their unlimited support. Many friends have helped me along the way by listening, offering advice and ideas. Special thanks go to my best friend and roommate, Omniyah Noory for supporting me during my ups and downs throughout this research. I would like also to thank my friend, Yasmin Adel for supporting me whenever I doubted myself. All efforts that have been made to keep our lab as an enjoyable and friendly place to work in, are appreciated and will be a memorable experience.

My deepest gratitude goes to my parents for their unlimited encouragement, endless support, and continuous love and prayers. I owe my parents, brother and sisters everything that I have learned or earned in my life. I know I can never come close to returning their favor upon me. May *Allah* reward them in this world and the Hereafter.

-Yara-

*To*

*My parents, Waleed and Amira,*

*My brother and sisters*

*The rest of my family,*

*And finally*

*To whom it may concern*

# CHAPTER 1

# INTRODUCTION

Existing distribution systems are designed to accept bulk power from the transmission network and distribute it to the loads. It is the utility's responsibility to generate, transmit and distribute the electricity to customers. This traditional structure is referred to as "centralized or regulated" electric power system. Though, it is generally agreed that the centralized electric power plants will remain the major source of electricity. However, centralized power plants face many challenges from different aspects such as high power loss, environmental pollution, and the need to update the energy infrastructure [1]. Over the last number of years, allowing small generation units known as distributed generators (DGs) to be connected at the distribution network is increasing significantly. This practice will move the conventional electric power plant from being regulated and centralized to deregulated power plants. Since distribution networks are designed without any generation at the customer side, integrating DGs into the distribution network can impact it positively or negatively.

This chapter presents the benefits and risks when connecting distributed generators to the existing distribution system. The chapter starts with an introduction on the structure of distribution networks and the concept of distributed generation. Then, the benefits of connecting DGs into distribution network and their impacts are presented. And lastly, an introduction to the islanding problem is given.

## 1.1 Conventional Electric Power Grid

Traditional power systems consist of four main Parts: Generation, Transmission, Distribution, and loads. In the generation phase, electricity is generally generated between 11 and 25 kV. Then, it is stepped up and transmitted via overhead lines from the generation units to remote areas of primary and secondary distribution systems

where the voltage is stepped down. Figure 1.1 shows the different phases and their voltage ratings [2].

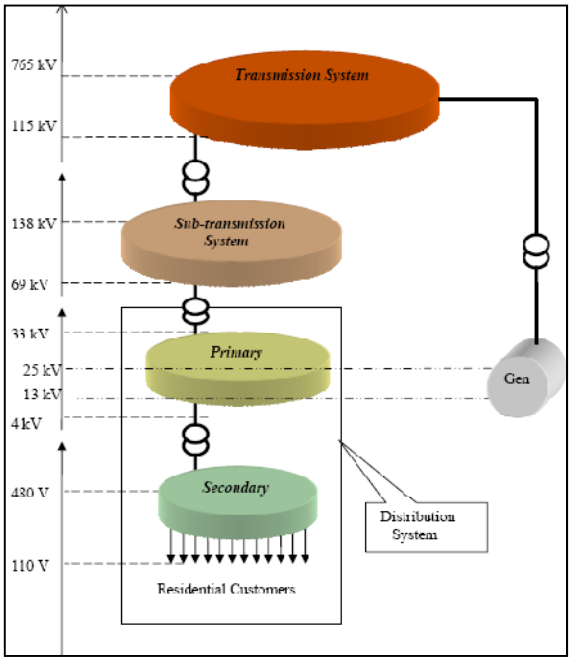


Figure 1.1: Different phases and their voltage rating in a traditional electric power grid.

## 1.2 Distributed Generators

A Distributed Generator (DG) is an electric power source of typically 5kW to 20MW capacity connected directly to the distribution grid away from the main substation [2]. Distributed Generators can be divided according to the electrical interfaces into two main classes: Rotating machines type and inverter based type.

- **Rotating machine DG type:**

DG of rotating type include synchronous and induction generators. The synchronous type includes reciprocating engines (diesel and gas), mini hydro, small gas turbine, and some wind systems. Induction generators include wind systems and reciprocating engines which run on fuel to generate electricity. The reciprocating DG type suffer from some drawbacks such as noise, emissions and maintenance cost [3].

- **Inverter based DG type:**

The inverter based DG type relies on the inverter to convert the electricity from the DG to a form that can be supplied to the distribution network. The inverter is actually an interface between the system and the generator, the structure of this

interface depends on the distributed generator type. DG could be rotating machine type or inverter based type as shown in Figure 1.2 [3]. If the source is a rotating machine operating at variable speed, such as those found in wind turbines and micro-turbines, the variable frequency AC voltage at the terminals of the generator is rectified and regulated to DC and then inverted to a fixed frequency AC current that is fed to the distribution network. On the other hand, if the distributed generation source has a varying DC voltage output, such as a photovoltaic array or fuel cell, the voltage may first be stepped up or down and pre-regulated by a DC/DC converter, or it may be fed directly to the DC to AC inverter. It is considered to be the most important functional block in the DG system since it is responsible for controlling the output active and reactive power of the DG.

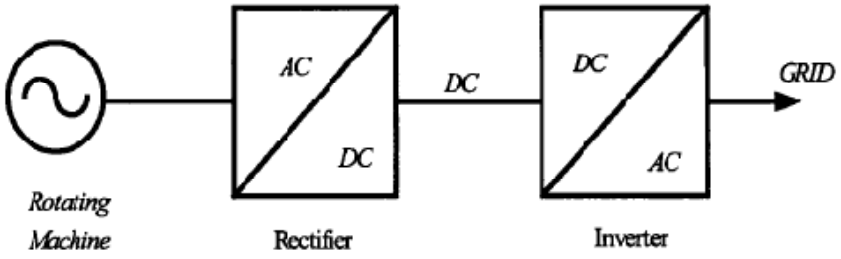


(a)

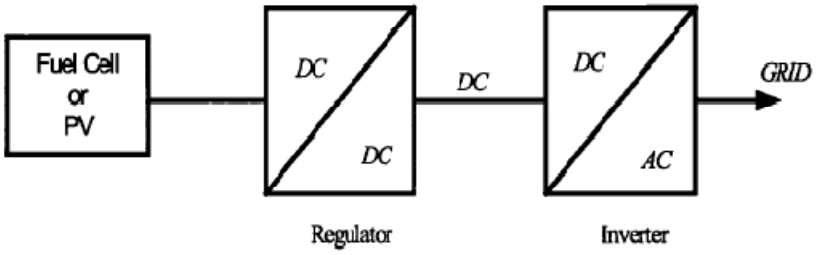


(b)

Figure 1.2: Inverter interface topology for (a) rotating machine (b) fuel cell or PV DG.

Environmental concern is now driving the use of renewable and clean energy. Photovoltaic power generation is expected to play a big part due to their small scale and low maintenance characteristics. According to Chinese electric power institute a total of 350MW is generated by installed PV panels. Moreover, it is expected that PV panel will account for a total of 1.8 GW by 2020 and 600 GW by 2050 [4].

Over the past two decades, PV efficiencies, reliability, and manufacturing capabilities have improved. As a consequence, the cost of photovoltaic panels has fallen significantly in the recent years and can be expected to continue to fall. The cost of PV panels has decreased by almost 70 percent since 1980 and is estimated to decrease by another 70 percent from current levels by 2020 as shown in Figure 1.3. Due to the various advantages of PV generation, the DG considered in this thesis is PV panels [5].

Distributed generator can be classified according to their technology into three main classes, namely, renewable, non-renewable and storage devices as shown in Figure 1.4.

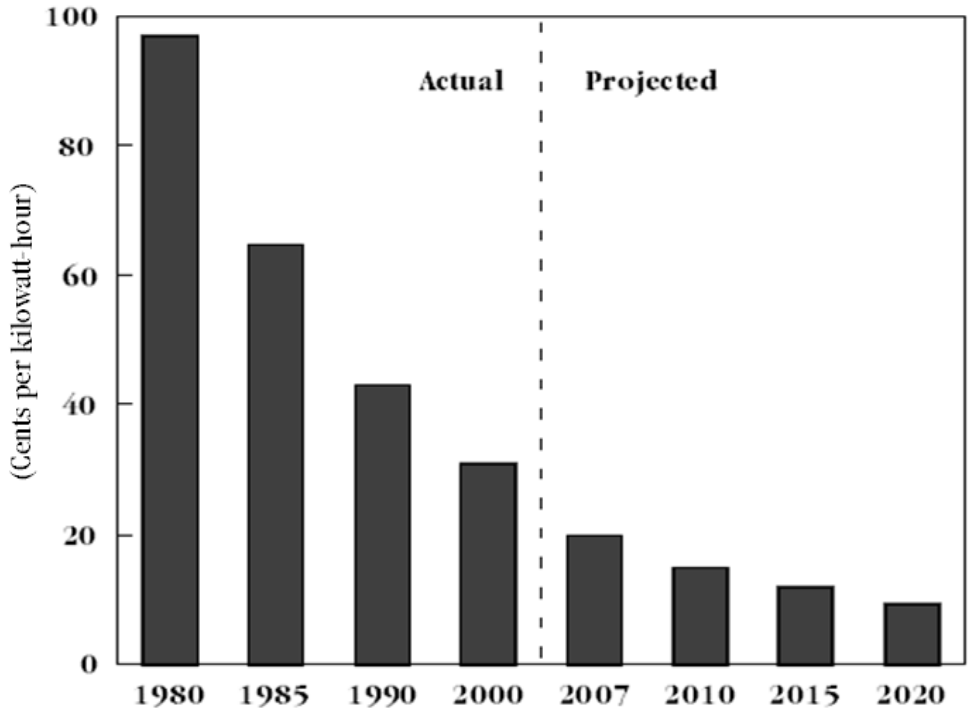


Figure 1.3: Cost of photovoltaic electricity.

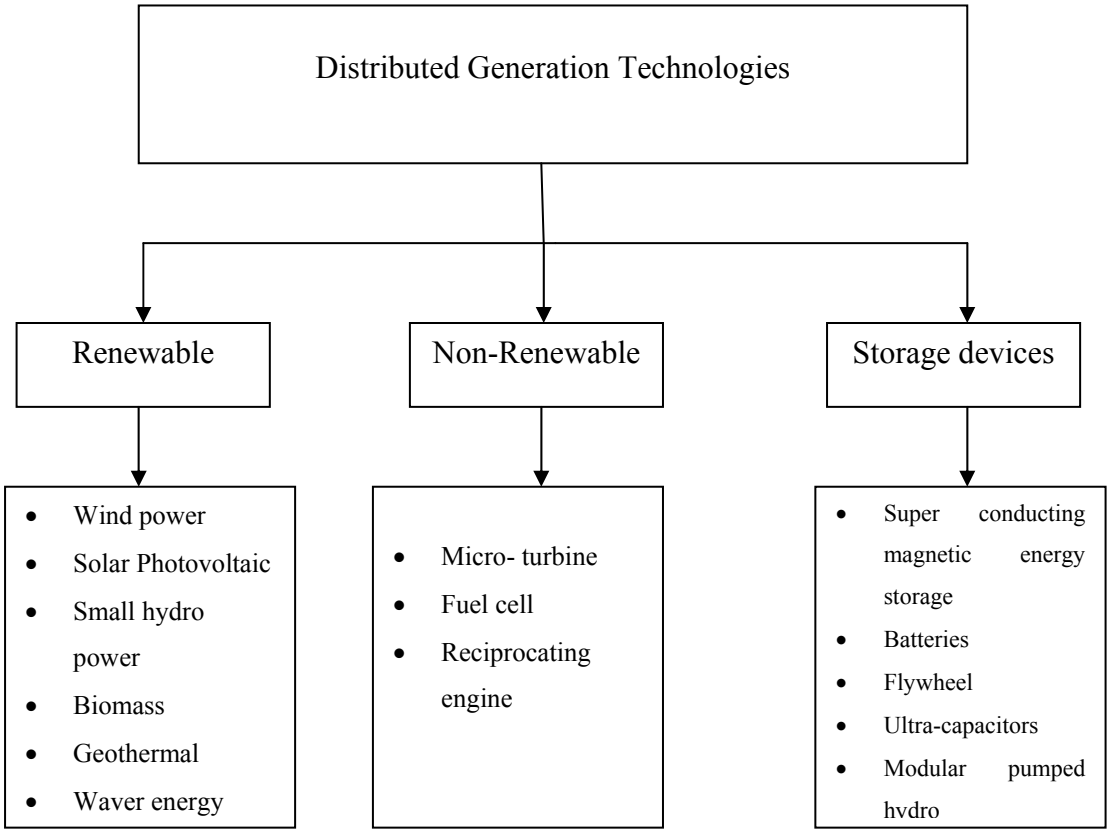


Figure 1.4: Distributed generation technology classification.

## 1.3 Benefits of Connecting DGs into Existing Distribution Network

Connecting DGs into the existing electric power grid has many benefits such as:

- *Power peak shaving*: Distributed generation operation during peak demand periods (Peak Shaving) contribute in supplying demand power during these high demand periods hence reducing the amount of electricity purchased during the peak price periods. In this way, distributed generation contributes in avoiding electricity price fluctuations. This is considered the major driver for distributed generation installation in US [1].
- *Network reliability:* Installing Distributed generators enhance the reliability of the system by providing a back- up in case of power interruption [1].

- *Voltage control:* Other than producing real power distributed generators provides reactive supply (absorption and injection) to achieve voltage control.

- *Power quality:* Distributed generation can assist in solving power quality problems, such as voltage sags, as the installation of a DG increase the voltage level in the network. Moreover, distributed generation can also contribute in the power factor correction [1].

- *Transmission and Distribution Deferral:* In some locations, where load goes beyond transmission line's capacity, addition of DG will be more economical than constructing distribution lines.

## 1.4 Technical Challenges when Connecting DGs into the Existing Distribution System

Distribution power systems are radial in nature. Power flows in one direction from the utility to the load. Most protection, monitoring, and control devices are designed based on this unidirectional flow of power. Hence, integrating distributed generators into the existing distribution power system will give rise to many problems such as: voltage regulation, fuse-recloser coordination, unintentional islanding, and increase the system's fault level [6]. Among all the above mentioned problems unintentional islanding is one of the most important concern when integrating DG into the grid [7].

Islanding phenomenon is the situation where the distribution system containing both distributed generator and loads is separated from the main grid as a result of several reasons such as electrical faults and their subsequent switching incidents, equipment failure, or pre-planned switching events like maintenance. Figure 1.5 shows a typical distribution system with three distributed generators connected to it [7]. Due to one of the reasons mentioned earlier circuit breaker "C" was tripped and a power island was formed.

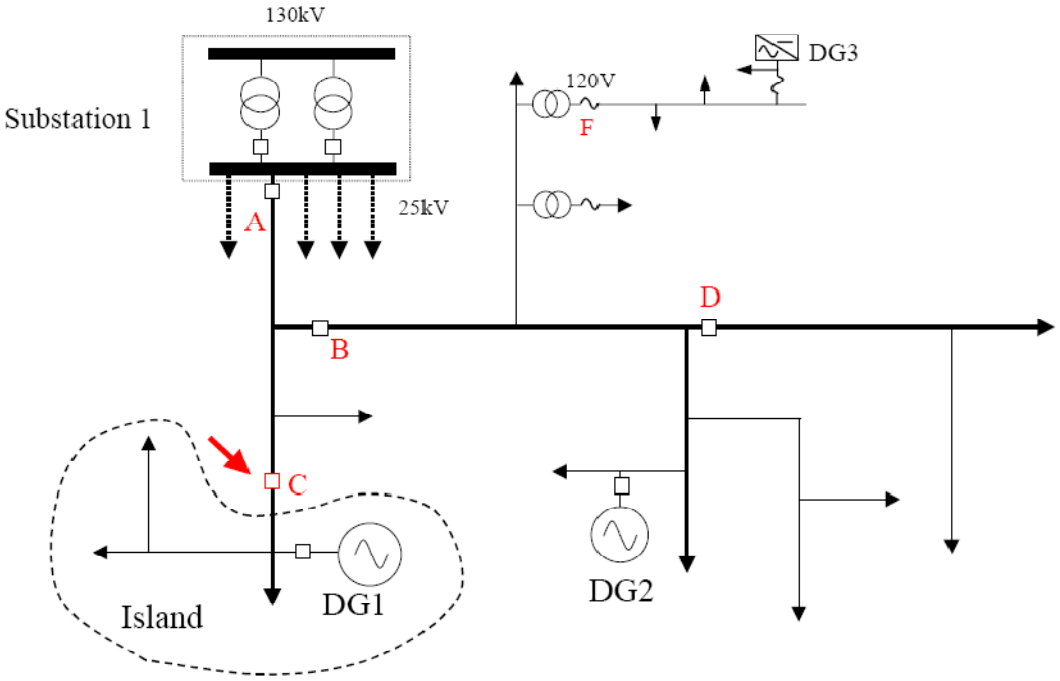


Figure 1.5 : Typical distribution system with distributed generators.

Unintentional islanding has the following implications on the electric power system.

- The voltage and frequency provided to the loads in the islanded system can vary significantly since the utility is no longer controlling the voltage and frequency, creating the possibility of damage to customer equipment [7].

- Islanding may create a hazard for utility line-workers or the public by causing a line to remain energized that may be assumed to be disconnected from all energy sources [7].

- The distributed generators in the island could be damaged when the island is reconnected to the grid due to the out-of-phase reclosing which can inject a large current to the generators. This is because the generators are likely not in synchronism with the system at the instant of reconnection [7].

For safe operation unintentional islanding should properly detected. According to IEEE Standard 1547-2003 and IEEE Standard 929-2000, DG units are normally disconnected from the AC line when the grid is not present [8].

## 1.5 Problem Statement

Presently, there are many methods which may be used to detect the islanding situation of DG(s). Passive methods such as under/over voltage and under/over frequency work well when there is an imbalance of power between the loads and the DG(s) present in the power island. However, these methods fail to detect the islanding condition if there is a balance of power supplied and consumed in the island. Various active methods which attempt to create a power imbalance so that the island may be detected also exist. However, these methods can degrade the quality of the power supplied by the DG and their ability to detect the island may be diminished when there are multiple DGs supplying power to the same island. The active methods may also require knowledge of the currents being drawn by the loads. Utility installed methods such as power line carrier communication require extra equipment and therefore may be expensive.

Attempts to use wavelet transform (WT) along with artificial intelligence as a technique to detect the phenomenon of islanding have been found in [9], [10] and [11]. However, these methods were implemented on rotating machine DG type. The method developed in [9] involved using the energy extracted from the current signal via WT as a feature vector in their pattern recognition model. On the other hand, the recurrent ANN based islanding protection technique used in [11] adopted the synchronous DG speed deviation as its feature vector.

Proposed is an islanding detection method based on implementing the wavelet transform of the voltage signal at the point of common coupling. A decision whether an islanding or not has occurred is obtained using the trained Artificial Neural network (ANN) model. A number of simulated voltage signals are acquired from the system modeled in PSCAD. The acquired voltage signals have mainly two classes: non-islanding and islanding. Simulated non-islanding cases include normal operation, temporary single line to ground (SLG), line to line to ground (LLG), and three phases to ground faults at different locations of the line on the distribution network, and switching of loads. On the other hand, the islanding cases simulated include opening of different circuit breakers which cause islanding at different times within one power cycle.

Wavelet analysis is a developed mathematical tool for signal processing. The basic concept in wavelet transform (WT) is to select an appropriate wavelet function "mother wavelet" and then perform analysis using shifted and dilated versions of this wavelet. In WT a windowing technique with variable-sized regions is used. Wavelet analysis allows the use of long windows where low-frequency information (approximation) is required, and short windows where high-frequency information (detail) is required.

The energy content of the detail coefficients for the voltage waveforms acquired are calculated for the obtained two different classes. A single arbitrary threshold is insufficient to discriminate between the different events. Therefore, the use of artificial intelligent technique is suggested. A well trained ANN has the capability of learning complex mapping, linear or nonlinear, from the input space to the output space.

The algorithm is modified in order to have the ability to detect the occurrence of islanding in real time implementation rather than offline monitoring. A real time implementation of the algorithm can be achieved using a sliding window. The algorithm starts by collecting a one cycle sampled data window for each signal. Then, a WT analysis is carried out and the energy content in the details of the obtained voltage waveforms are calculated. Then a sliding data window as mention earlier is used, i.e., for each new sample to enter the window the oldest one is disregarded and the algorithm starts. A decision will be made whether an islanding has taken place or not using ANN.

## 1.6 Thesis objectives and contribution

The capabilities of some conventional passive islanding detection techniques are verified using computer simulation. The techniques considered in this thesis are under/over frequency (UOF), under/over voltage (UOV) and detection of harmonics (DH). It was found that UOF and UOV passive methods fail to detect islanding if the power generated is matched with the power consumed by the load. On the other hand, DH has the problem of false tripping since it is hard to set an appropriate threshold that provides islanding detection. Therefore, these passive techniques are not capable of detecting islanding alone and they should be combined with other techniques especially in the presence of multiple DGs in the distribution network.

The main objective of this thesis is to design reliable, fast, and cost effective islanding detection approach which work well in case of matched power situation and in the presence of multiple DGs. Another objective is to select an appropriate discriminative feature which will successfully detect islanding.

Proposed is a Neuro-wavelet based islanding detection technique in which the voltage signal at the PCC will be acquired and then decomposed into different frequency bands using DWT. The energy content of the wavelet details will be calculated and fed to a trained ANN. A decision whether an islanding or non-islanding event will be obtained using the trained ANN.

The proposed method has the potential to detect islanding conditions reliably in the presence of multiple DG islands. It is based on local cost effective measurements. Moreover, it is fast as the islanding detection time is less than 2 seconds which is the allowed detection time according to the IEEE standards. In addition of being fast and cost effective, the proposed technique has no negative impact on the power quality unlike proposed active techniques.

## 1.7 Thesis outline

The thesis is organized in 5 chapters as described below:

Chapter 2 presents a literature review on the previous work conducted in the area of islanding detection. The principle of operation, the benefits, and the drawbacks of each method are discussed.

Chapter 3 deals with the performance of UOF, UOV and DH passive techniques. It begins with the theory behind these passive techniques and a detailed description of the system model used for all the simulations in this work. The results of the implemented techniques are then presented and discussed to show the limitations of those techniques.

In chapter 4 the proposed neuro-wavelet based islanding detection technique is fully described. The chapter gives an overview of artificial neural network (ANN) architecture. The training process of ANN is then explained. A detail description of wavelet transform is then presented. The methodology of the proposed technique is fully explained. Finally, simulation test results showing the proper operation of neuro-wavelet technique are presented and discussed.

Chapter 5 concludes and summarizes the important contributions and findings of the proposed neuro-wavelet base islandind detection technique. Specific recommendations regarding islanding detection in multi-DG islands and for the implementation of a neuro-wavelet based islanding detection scheme are presented. Finally, suggestions for future work are identified.

# CHAPTER 2

# ISLANDING DETECTION

A critical requirement for grid connected DG is islanding detection. According to IEEE std. 1546, the DG should be disconnected once an islanding event is declared. Several islanding detection techniques have been proposed in the literature. An overview of various islanding detection methods, principles of operation, their strengths and drawbacks are introduced in this chapter.

## 2.1 Review of Established Islanding Detection Methods

Islanding detection methods may be divided into two main categories: remote methods and local methods. Remote techniques are based on the communication between the utility and the distributed generators. On the other hand, local techniques are based on the data available on the distributed generator side. Local techniques can be further classified into passive and active methods [12] as shown in Figure 2.1.

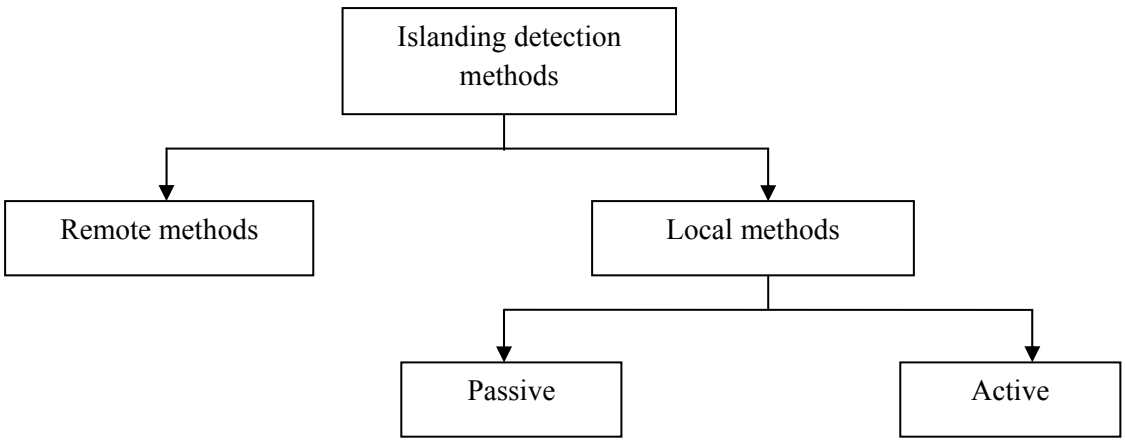


Figure 2.1: Classification of islanding detection methods.

An islanding detection method may have a non-detection zone (NDZ). The NDZ is mainly associated with a range of active and reactive power ($\Delta P, \Delta Q$) in which the detection method fails to detect the occurrence of an island. A positive $\Delta P$ indicates an excess of the power consumed by the load within an island resulting in under voltage. On the other hand, a positive $\Delta Q$ indicates an excess of reactive power consumed by the load resulting in an over frequency. A small mismatch in the active and reactive power will not be sufficient to cause tripping of voltage and frequency relays which will be fully discussed in chapter three. An accepted way of comparing and evaluating two anti-islanding detection techniques is by comparing the area of the NDZ. A method resulting in a smaller NDZ will be able to detect the islanding more reliably. Figure 2.2 shows an example of NDZ; the shaded area shows the active and reactive power mismatch regions in which the method will fail to detect islanding events.

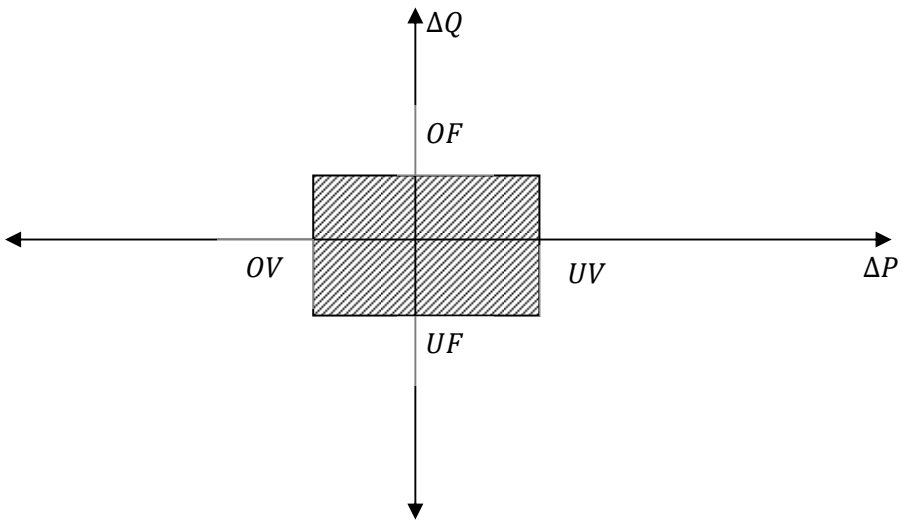


Figure 2.2: An example of non-detection zone.

### 2.1.1 Passive methods

Passive methods basically monitor selected parameters such as voltage and frequency in order to decide whether or not an islanding has taken place. Passive methods are easy to implement and consist of equipment installed on the DG side. Under/over frequency (UOF), under/over voltage (UOV), detection of harmonics (DH) and phase jump detection (PJD) are the common used passive techniques. The performance of these techniques will be explained in the following section.

#### 2.1.1.1. **Under/Over voltage and Under/Over frequency**

All grid-connected PV inverters are required to have under/over frequency protection methods (UOF) and under/over voltage protection methods (UOV). These UOF/UOV protective devices protect the customer's equipment and used also as an anti-islanding detection methods.

Consider the system configuration shown in Figure 2.3 in which a photovoltaic panel is connected to the grid. Node 'a' is the point of common coupling between the utility and PV panel. When the utility is connected, real and reactive power ($P_{pv}$+j$Q_{pv}$) will be supplied from the DG. If the power rating of the load is greater than that of the DG then the power mismatch ΔP, Δ Q will be compensated from the grid. However, when the grid is disconnected and an island is formed, the voltage and frequency will deviate. The behavior of this method will depend on ΔP and ΔQ. If $\Delta P \neq 0$ then the amplitude of the voltage at PCC will change and the UOV protective relay will detect the islanding. Similarly, if $\Delta Q \neq 0$ then the phase of the voltage at the PCC will deviate resulting in frequency deviation which will be detected using UOF protective relays. If ΔP and ΔQ are large enough the voltage and frequency will go beyond the nominal ranges of UOF/UOV protection devices and a trip signal will be sent to trip circuit breaker CB2.

This method will fail to detect islanding if the load is closely matched to the inverter's output power. The voltage and frequency deviation will not be sufficient to exceed the nominal ranges of UOF/UOV protection devices.

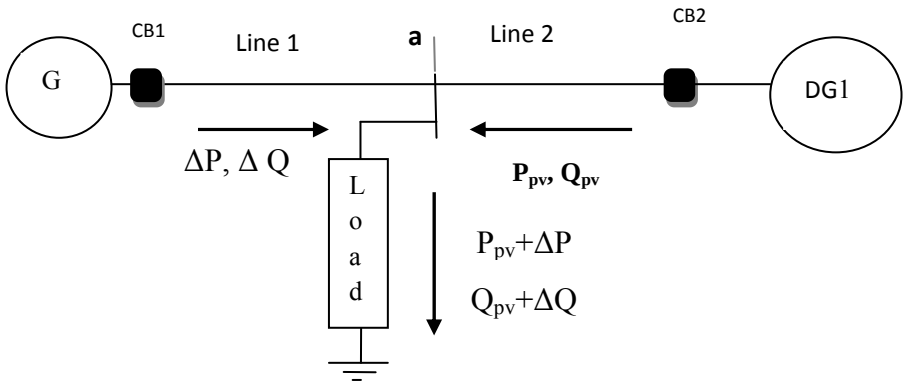


Figure 2.3: Distribution system with Photovoltaic DG.

#### 2.1.1.2. **Detection of Harmonics**

There are several ways to calculate the harmonic content in a voltage or current signals. The most common way is to calculate the total harmonic distortion (THD) which is calculated according to equation (2.1):

$$THD = \frac{\sqrt{\sum_{h=2}^{N}\left(V(h)\right)^2}}{V(1)} \tag{2.1}$$

Where: $V(h)$ is denoted for all the harmonic components except for the fundamental and $V(1)$ is the fundamental frequency component.

There are two main sources of harmonics in typical distribution systems. The first source includes power electronic converters such as three phase inverter while the second source includes devices that exhibit non-linear relationship between the voltage and current such as transformers.

This method involves monitoring the THD of the voltage or current signal at the point of common coupling. During grid connected mode, the distorted current which includes the harmonics will flow from the inverter out to the utility since the grid has lower impedance compared to that of the load. The current containing the harmonics will interact with the low impedance grid producing small amount of distortion in the voltage signal. However, when the grid is disconnected, the current containing the harmonics will be forced to flow into the load which has high impedance producing larger amount of distortion in the voltage signal compared to the amount produced under grid connected mode. If the THD was large enough it will exceed the threshold and islanding will be detected.

#### 2.1.1.3. **Phase jump detection**

This method involves monitoring the phase difference between the voltage and the current of the DG's output for a sudden jump. Under normal condition and for current source inverters, the inverter's output current which will be synchronized with the utility voltage by detecting the rising or falling zero crossing for synchronizing purposes. This can be achieved using a phase locked loop (PLL). In case of islanding,

the inverter's current is fixed by the utility voltage source since it is following the template provided by the PLL but the voltage is no longer fixed. The phase angle of the load should be maintained to that before the disconnection. In order to achieve this condition, the voltage will "jump" to this new phase. The phase error is measured and once it exceeds certain threshold islanding is detected. Figure 2.4 shows the operation of voltage phase jump detection method [12].

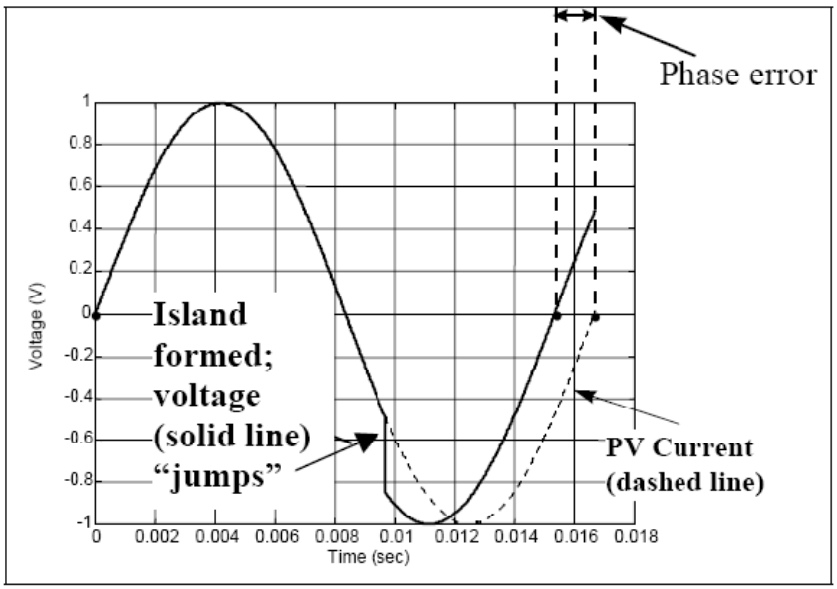


Figure 2.4: Operation of voltage phase jump detection method.

#### 2.1.1.4. **Other passive detection methods:**

Other passive detection methods were proposed. These methods include voltage unbalance [8], comparison of the rate of change of frequency (ROCOF) [13], and monitoring the voltage and changes in power factor [14].

Passive methods in general are easy to implement. Unfortunately, the majority of these methods suffer from large NDZ which is due to the difficulty to choose a suitable threshold on the monitored parameters. This threshold should be capable of differentiating between an islanding condition and any other disturbances in the system to avoid false tripping.

### 2.1.2 Active methods

Active methods basically introduce disturbances to the connected circuit and then monitor the response of the system to determine whether or not an islanding has occurred. Active methods involve some kind of feedback or control mechanism that force the system‘s frequency or voltage at the point of common coupling to deviate outside the acceptable limits such that islanding maybe detected using passive UOF and UOV. During the grid connected operation the frequency and voltage of the DG will be controlled by the utility. However, during islanding operation the DGs are in control of the power island and the deviation from nominal values will occur. This section will briefly describe some implemented active methods.

#### 2.1.2.1. **Slip mode frequency shift**

Slip mode frequency shift method (SMS) involve using positive feedback to detect islanding. Positive feedback can be applied to the voltage, frequency or phase of the voltage at the point of common coupling. In this method a positive feedback is applied to the phase of the voltage at the point of common coupling. The phase angle between the terminal voltage and the DG current is a function of the frequency deviation.

Normally, PV panel tend to operate at unity power factor hence the phase different between the DG voltage-current output is controlled to be equal to zero. However in SMS the phase angle is controlled to be a function of the frequency of the voltage signal at PCC. Under grid connected condition, the frequency is fixed and stabilizes at 60 Hz. Once the utility is disconnected, the frequency deviates and the phase angle changes. This positive feedback mechanism results in frequency instability and derive the system to operate at new frequency which will be detected by UOF protective relay [12].

#### 2.1.2.2. **Active frequency drift**

Active frequency drift (AFD) can be easily implemented with a microprocessor-based controller. In AFD, the DG output current injected to the utility is slightly distorted. In this case there is a continuous tendency to drift the frequency. Figure 2.5 shows an example of the distorted DG output current waveform along with undistorted sine waveform for comparison [12].

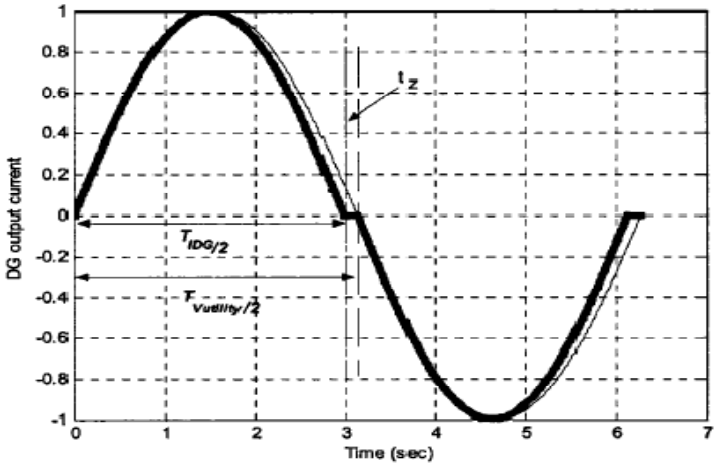


Figure 2.5: DG output current using AFD.

When the utility is connected it is impossible to change the frequency. However, when the utility is disconnected, the frequency at the PCC will drift up or down seeking the load resonant frequency. This process continues until the frequency deviation will be detected using UOF passive devices. Though AFD is easy to implement, it intentionally introduces a distortion in the system which will result in power quality degradation.

#### 2.1.2.3. **Sandia frequency shift**

Sandia frequency shift method (SFS) is an extension to the AFD method. In this method a positive feedback is applied to the frequency and the voltage at the point of common coupling. During normal operation the presence of the relatively strong utility source should overpower the positive feedback of the SFS equipped DG resulting in stable operation. However, during the absence of the utility, the DG is in control of the system frequency. The SFS aims to force the system frequency outside the acceptable limits. The error in the system frequency is multiplied by a gain greater than zero and then added to the actual system frequency. This sum is used as the frequency of the DG's output. This means that the system frequency is unstable and should quickly rise or fall outside the operating limits of the passive relays [15]. SFS is easy to implement and has small NDZ compared to other active techniques. However, it has negative impact on the power quality since the instability of the DG inverter's output can cause undesirable transient behavior when a weak utility is connected. This problem will be duplicated as the penetration level of DG into the network increases.

#### 2.1.2.4. **Other active detection methods**

Some other active detection methods were proposed. An active method based on negative sequence current injection was proposed in [16]. Reactive power insertion method which is applicable to synchronous machines and inverter based DG but not for induction machines was presented in [17]. A hybrid islanding detection technique for synchronously rotating DGs is introduced in [8]. The technique combined both the positive feedback (PF) technique (active method) and voltage unbalance and total harmonic distortion (VU/THD) technique (passive method). Simulation results show that the proposed hybrid technique is more effective than each of the techniques used alone.

An alternative islanding detection technique suitable for inverter interfaced generators based on the correlation principle is proposed in [15]. A correlation islanding detection technique, which operates based on the correlation between disturbances in system voltage and a pseudo-random sequence used to perturb the generator's output was developed. The performance of the system when using three different pseudo random sequences (Maximal length, kasami and gold sequences) was studied. It was found that gold sequences have better performance than maximal length and kasami sequences.

In general active islanding detecting methods have smaller NDZ than the passive islanding methods. During matched power condition between the DG output power and the load, injecting disturbances into the system results in a mismatch power condition and islanding can be detected. However, in a mismatched power condition injecting disturbances into the system may coincidentally create a matched power condition and the method fails to detect the islanding. Although active methods provide more reliable islanding detection than passive methods, they have negative impact on the power quality of the system in the grid-connected mode. This could be duplicated if the penetration level of the DGs in the network increases. Under specific conditions, the injected signal for islanding detection may even result in instability of the system in a grid-connected mode.

### 2.1.3 Remote methods

Remote islanding methods are communication based methods. Islanding is detected based on the status of the utility circuit breakers. In communication based methods, each DG site has a receiver, and all the circuit breakers in the line leading to the DG site from the utility have transmitters. The state of the circuit breaker is monitored and a signal is then sent to trip the DG unit in case of islanding [12].

#### 2.1.3.1. **Power line carrier communication**

Power line carrier communications (PLCC) involves sending a low energy communications signal along the power line itself. Figure 2.6 shows a system configuration using PLCC anti-islanding method [10]. A receiver is installed on the customer side of the point of common coupling. A PLCC transmitter located at the utility sends a signal along the power line to the receiver to perform a continuity test of the line. The receiver on the customer side will detect the presence or the absence of the signal. If the PLCC signal disappears, this indicates an islanding event since there is a break in the continuity of the line and the PLCC signal is lost [12].

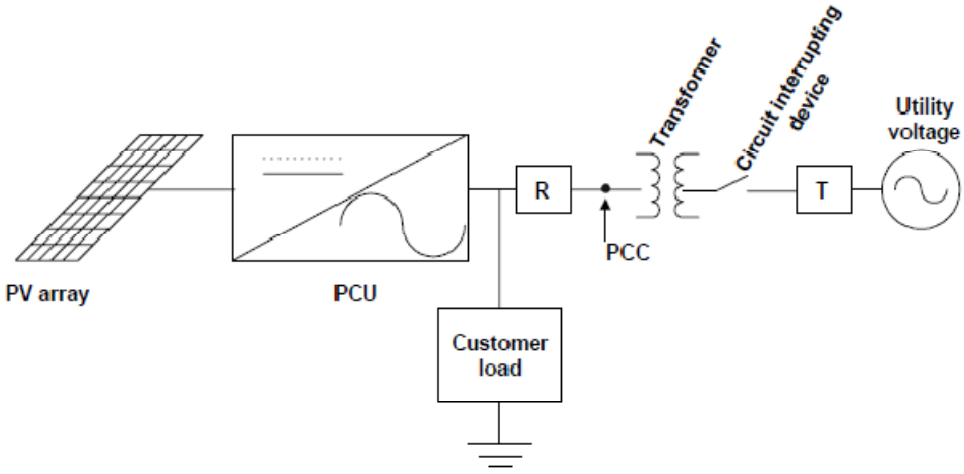


Figure 2.6: System Configuration Including a PLCC Transmitter (T) and Receiver (R).

#### 2.1.3.2. **Signal produced by disconnect**

The signal produced by disconnect (SPD) method is similar to the PLCC method. However, in SPD method the signal is not transmitted using the power line. Instead, the utility recloser is equipped with a small transmitter that sends the signal to the DG when the recloser opens via microwave link, telephone line, or other means. In this method the state of the switch is directly communicated to the DG [12].

Though these techniques do not have NDZ and more efficient than both passive and active methods but they are expensive and complex to implement and hence non popular.

### 2.1.4 Artificial intelligence based techniques

Another method with the potential to detect islanding in case of matched power is proposed in [9]. The studied system contains two DGs. The DGs were synchronous machine and induction machine. The method involves using pattern recognition techniques to recognize the transient patterns produced from the islanding events. The discrete wavelet transform was used to extract the energies of the current waveform at the point of common coupling. Then the energies were adopted as a feature vector to train the pattern model. The performance of three different pattern classifiers was studied. The three classifiers are: decision tree making, probabilistic neural network and support vector machine. Each trained classifier was then tested with novel test current waveforms. It was found that decision tree classifier resulted in the best performance.

An intelligent based approach for detecting islanding was introduced in [10]. The technique uses 11 features to classify any possible islanding event. A decision tree approach was adopted to classify the islanding events. The technique was tested and on a real system with multiple DGs and the results indicated that the approach can detect islanding event with good degree of accuracy.

In another study, a recurrent artificial neural network based islanding protection technique is proposed in [11]. The feature vector used is the synchronous generator speed deviation.

### 2.1.5 Signal processing based techniques

A wavelet transform-based islanding detection algorithm for inverter-assisted distributed generators is proposed in [19] and [20]. A discrete wavelet transform of the signals using Daubechie's mother wavelet and scaling function at the fifth level were used. The voltage signal at point of common coupling and the inverter current were analyzed. The wavelet power which is the product of the voltage wavelet detail coefficients and the current wavelet detail coefficients are calculated. The wavelet power is then compared to an adaptive threshold. This adaptive threshold can be

achieved using fuzzy logic threshold controlled which used the RMS value of the voltage at PCC, inverter's current and wavelet power and set a threshold based on the load. Since the threshold is dependent on load so it can also be considered to be fuzzy.

The simulation results proved that the proposed method works with loads having quality factor greater than 2.5. A result with nonlinear loads shows the effectiveness of this method. The proposed algorithm also distinguishes between islanding and any other transients in power systems [19]. Though the proposed technique has the potential to detect islanding, it was tested on single phase diagram. However, for three phase system, all the phases need to be monitored. Moreover, the proposed technique was tested on single DG. Also the proposed algorithm needs to be tested for multiple inverter case.

# CHAPTER 3

# LIMITATIONS OF PASSIVE ISLANDING TECHNIQUES

The performances of the most widely used passive anti-islanding detection methods are evaluated analytically and verified by computer simulation. These techniques are under/over frequency (UOF), under/over voltage (UOV), and detection of harmonics (DH) passive anti-islanding schemes. The computer simulation of the system model followed by the principle of operation for each scheme is explained.

## 3.1 System Model

The performances of the islanding detection schemes are tested on a system model simulated by PSCAD 4.2 from Manitoba HVDC research center. The model simulated is adopted from [15] and is based on a data from a real system. The modeled circuit is the same as the anti-islanding testing circuit defined in UL 1741 (Standard for Inverters, Converters, Controllers and Interconnection System Equipment for Use With Distributed Energy Resources) and IEEE 929 [21]. The testing circuit consists of an AC power supply to emulate the grid and a test load that remains connected to the near DG when an island is created. The system model diagram is shown in Figure 3.1.

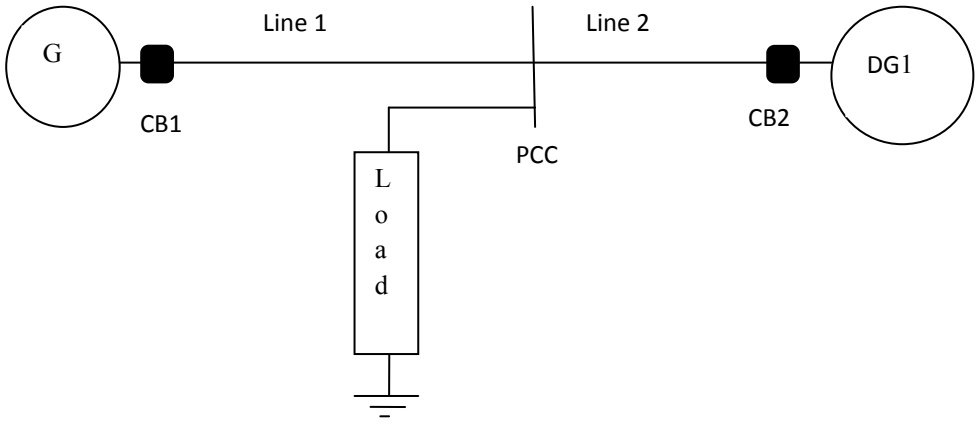


Figure 3.1: System model.

The testing procedure requires that the active and reactive power supplied from the DG match the power required by the test load. Because the load is very close to the DG compared with the grid, almost all the power required by the load is taken from the DG. Therefore, when islanding takes place, the detection is difficult. According to the previously mentioned standards much of work has been done to define the testing load. It is generally agreed that an RLC load tuned at the line frequency gives the worst case representation of an island. Other loads (i.e. transformers or non-linear loads) are less likely to create a non-detectable island or their effect could be duplicated with an RLC load [7]. The PSCAD model under study is shown in Figure 3.2 and the system data is found in Table 3.1. Detailed description of the system model elements is given in the following subsections and the PSCAD simulation figures are attached in APPENDIX A.

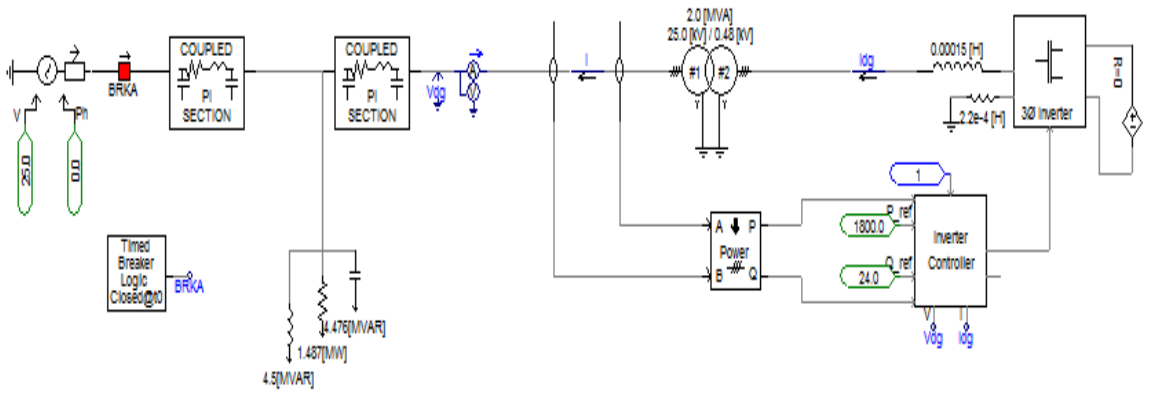


Figure 3.2: PSCAD simulated system model.

Table 3.1: System parameters

| Parameter | Value | Line Parameter | Value |
|---|---|---|---|
| $V_{source}$ | 25kV | Length 1 | 10 km |
| $Z_{source}$ | 6.45+j14.4 Ω | Length 2 | 1 km |
| $R_{load}$ | 347 Ω | $R_1$ | 0.2138 Ω/km |
| $L_{load}$ | 0.368 H | $R_o$ | 0.3875 Ω/km |
| $C_{Load}$ | 19.09 μF | $X_1$ | 0.3928 Ω/km |
| DG TX ratio | 25/0.48 | $X_o$ | 1.8801 Ω/km |
| DG TX X1 | 6% | $B_1$ | 4.2315 μS/km |
| | | $B_o$ | 1.60585μS/km |

### 3.1.1 Utility Source

The utility source of the system under study is a 25kV substation. It is modeled as an ideal 25kVsource behind an impedance of $6.45 + j14.4\ \Omega$. Islanding is achieved by opening of circuit breaker BRKA.

### 3.1.2 Lines

There are two sections of line in the model. The first line connects the substation to the load bus and is 10km long. The second line connects the load bus to the DG and is 1km long. Both lines have the same impedance per kilometer. Since both lines are relatively short, pi sections are suitable for modeling them at the power system frequency.

### 3.1.3 Load

In this study, a parallel RLC load is selected to test the islanding detection method. The resonant frequency of the load which is defined as in (3. 1) should be equal to the grid line frequency (60 Hz in this study).

$$f = \frac{1}{2\pi\sqrt{LC}} \tag{3.1}$$

Where: $f$ is the grid frequency in Hz; $L$ is the effective load inductance in Henry; and $C$ is the effective load capacitance in Farad. Additionally, The quality factor ($Q_f$) calculated according to (3.2) is selected to be 2.5. The higher the quality factor the stronger the resonance. In such case it is difficult to drift the frequency of the islanded system.

$$Q_f = \frac{\sqrt{Q_L \times Q_C}}{P} \tag{3.2}$$

Where: $Q_L$ is the inductor reactive power; $Q_C$ is the capacitor reactive power; and $P$ is the active power. Mathematically, the load can be calculated according to the following equations:

$$R = \frac{V^2}{P} \tag{3.3}$$

$$L = \frac{V^2}{2\pi f \times Q_f \times P} \tag{3.4}$$

$$C = \frac{Q_f \times P}{2\pi f \times V^2} \tag{3.5}$$

The load is modeled as a parallel RLC load. The load is 2MVA with a power factor close to unity. It is modeled using a 1.8MW wye connected resistive load (R=347 at 25kV) in parallel with a 4.5 MVAR inductive load (L=0.368H at 25kV, 60Hz) and a 4.476MVAR capacitive load (C=19.09μF at 25kV, 60Hz).

### 3.1.4 Distributed Generator

The DG studied in this work is photovoltaic panel (PV). It can be modeled as a typical three phase inverter with a series inductor as an output filter. The inverter is current controlled. In case where more than one DG is connected to the system all the DGs are implemented identically. The individual components of the DG are described in detail below.

#### (a) Inverter

The Inverter is modeled using the standard three phase three leg inverter topology shown in Figure 3.3. The DC side voltage is taken to be a constant 900V.

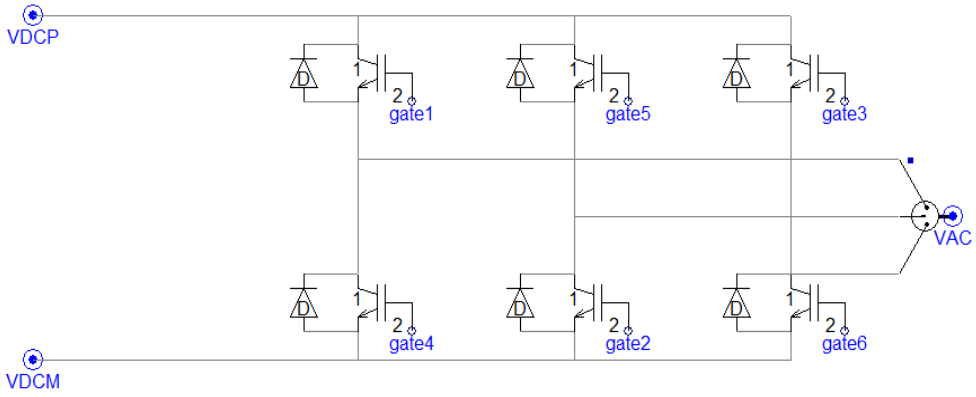


Figure 3.3: PSCAD model of a Three phase inverter.

**(b) Inverter Controller**

The DG inverter interface shown in Figure 3.4, is current controlled. It is implemented using PSCAD existing components. The frequency and phase of the system is determined using phase locked loop (PLL) of the point of common coupling voltage.

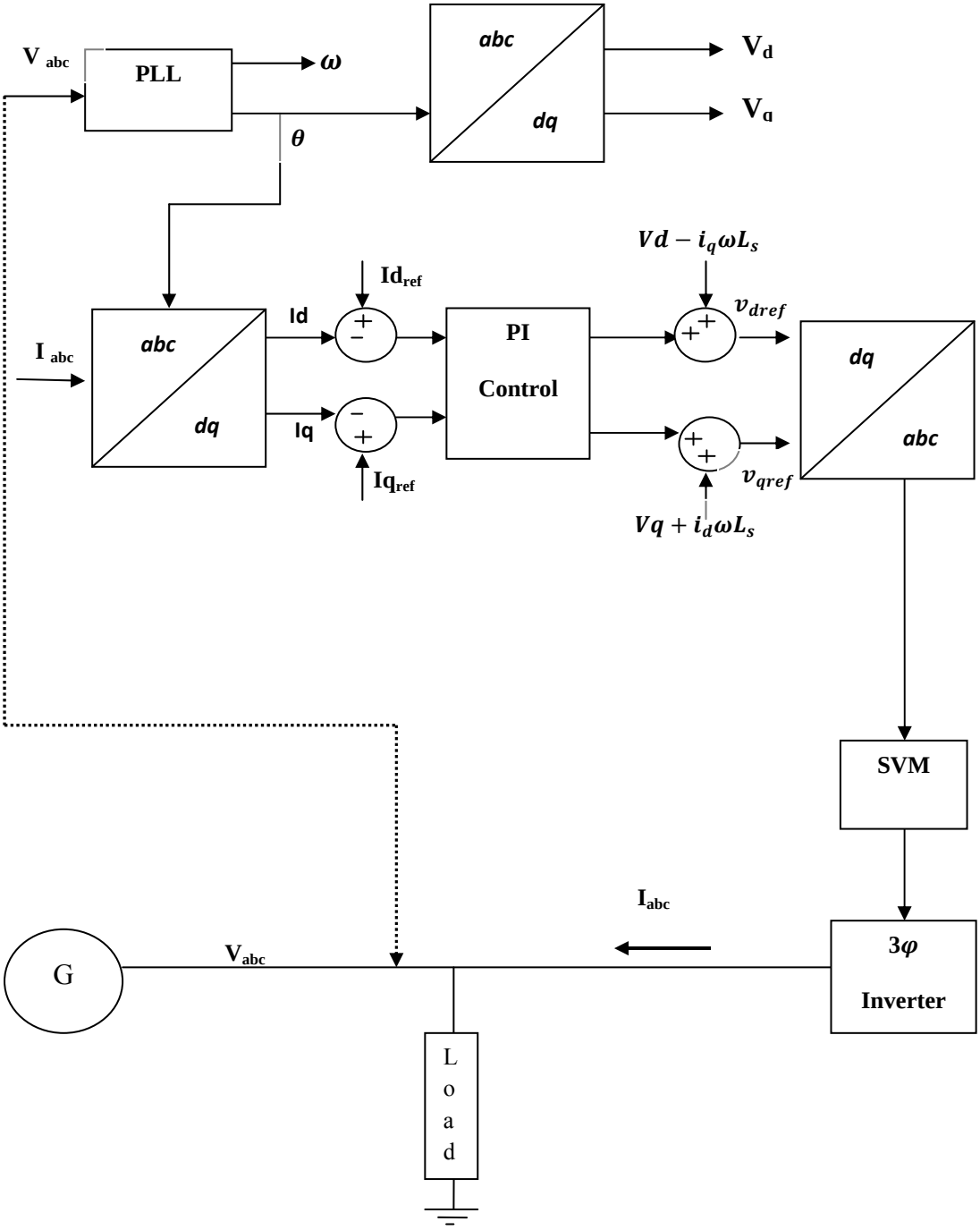


Figure 3.4: Inverter current controller.

The *abc* voltage components are then transferred to the *dq* components according to (3.6) which is referred to Park transformation.

$$V_{abc} = \sqrt{\frac{2}{3}} \begin{bmatrix} \cos(\theta) & \sin(\theta) & \frac{1}{\sqrt{2}} \\ \cos(\theta - \frac{2\pi}{3}) & \sin(\theta - \frac{2\pi}{3}) & \frac{1}{\sqrt{2}} \\ \cos(\theta + \frac{2\pi}{3}) & \sin(\theta + \frac{2\pi}{3}) & \frac{1}{\sqrt{2}} \end{bmatrix} \begin{bmatrix} V_d \\ V_q \\ V_o \end{bmatrix} \quad (3.6)$$

Similarly, the abc current components are transferred to the dq components using (3.6). Since the goal of this work is to detect islanding when the power within the island is matched to that of the load, it is desirable for the DG controller to accept the desired active and reactive powers, rather than currents, as the reference signals and converts them to the corresponding current reference using (3.7).

$$Id_{ref} = \frac{P_{ref}}{V_d}\ ,\ Iq_{ref} = \frac{Q_{ref}}{V_d} \quad (3.7)$$

There exist constant power controllers such as those implemented in [22] and [3]. Constant power controller is more complex than constant current controller since it uses twice as many gains to select. The performance of the controller selected was sufficient to achieve persistent islanding without the additional complexity of the control strategy [15].

The outputs of the PI controllers ($V_{dref}$ and $V_{qref}$) are then processed to obtain the modulation signal amplitude and phase angle. A space vector modulation (SVM) scheme is used to determine the gating signals to the three phase inverter.

**(c) UOF protective relay**

A component was created with a single input, the system frequency which is measured by the PLL, and a single output, a trip signal. The relay is provided with timers which are used to delay tripping in order to avoid false tripping in the case of transient deviations from the nominal frequency (i.e. switching). The frequency

settings are chosen according to the IEEE interconnection standards prescribed to response to abnormal system frequencies shown in Table 3.3 [15].

**(d) UOV protective relay**

UOV protective relay is designed with the help of the online Fast Fourier Transform (FFT) block available in PSCAD and shown in Figure 3.5. FFT block determines the root mean square (RMS) harmonic magnitude and phase of the input voltage signal as a function of time. The on-line frequency scanner allows the user to chose the number of harmonics from n=7 up to 255. The voltage settings are chosen according to the IEEE interconnection standards prescribed to response to abnormal system voltages found in Table 3.2. The protection device is provided with counter which will trip the system after the allowed maximum trip time passes. For example if the measured RMS voltage was between 50 and 88% of the nominal voltage, the relay will send a trip signal if the condition was satisfied for the consecutive 120 cycles according to the IEEE interconnection standards.

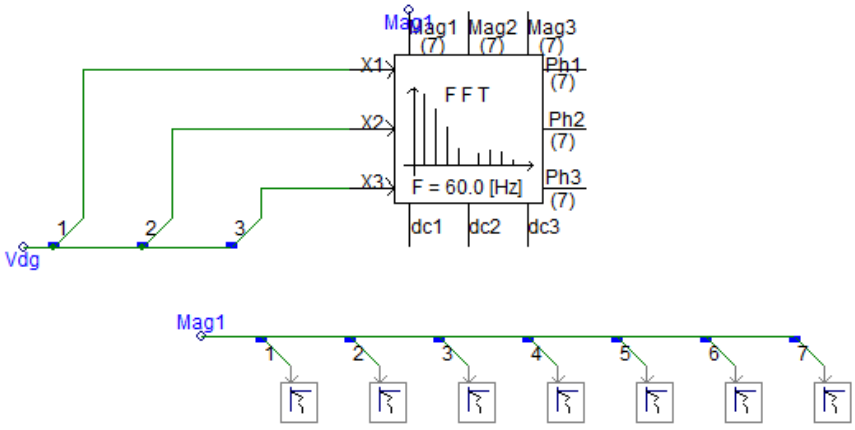


Figure 3.5: FFT block in PSCAD.

### 3.1.5 Total Harmonic Distortion Calculations

The total harmonic distortion (THD) for the inverter output current can be obtained using the built in PSCAD blocks shown in Figure 3.6. The total harmonic distortion component measures both the total and individual harmonic distortion of the inverter's output current signal according to (3.8):

$$THD = \frac{\sqrt{\sum_{h=2}^{N}\left(V(h)\right)^2}}{V(1)} \tag{3.8}$$

The greater the number of frequency components used ($h$) the more accurate the THD estimation will be. However, the simulation will take longer time to run. The number of frequency components is taken to be 255.

According to the IEEE interconnection standard the THD of the inverter's voltage at PCC should be kept under the 5%.

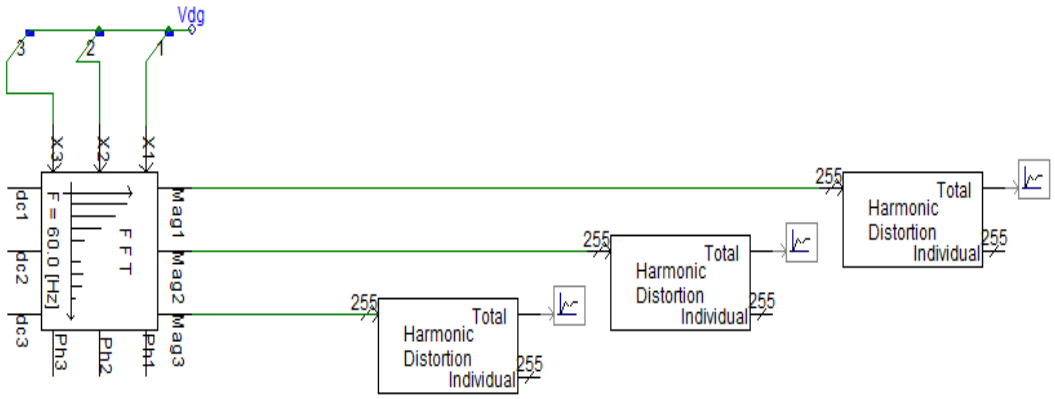


Figure 3.6: THD calculation of the inverter output current in PSCAD.

## 3.2 UOF/UOV Principle of Operation and simulation results

UOF/UOV Passive methods basically monitor the system's voltage and frequency in order to decide whether or not an islanding has taken place. They are easy to implement and consists of UOV/UOF protective relays installed on the DG side as discussed in section 3.1.4. Figure 3.7 shows the generic system for anti-islanding.

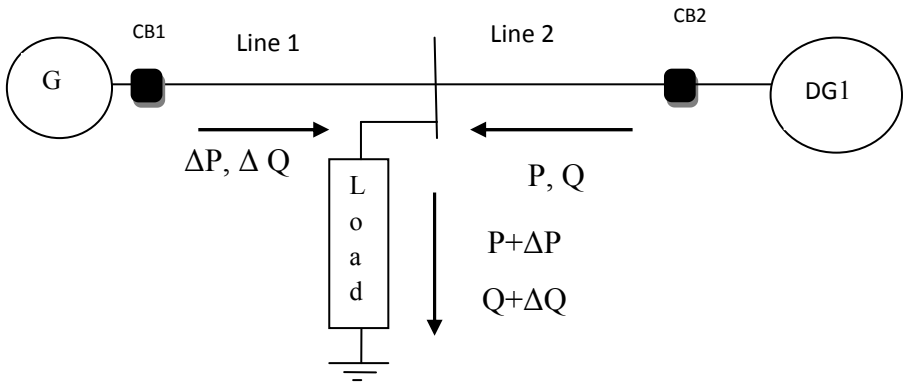


Figure 3.7: System under study.

The DG will supply the active and reactive power needed for the load. In practical conditions, some power mismatch exists between the DG output and the load i.e. $\Delta P \neq 0$, $\Delta Q \neq 0$. During the grid connected condition, the power mismatch will be compensated from the grid. However, when the grid is disconnected and an island is formed, the voltage and frequency will deviate. If $\Delta P$ and $\Delta Q$ are large enough the voltage and frequency will go beyond the nominal ranges of UOF/UOV protection devices and a trip signal will be sent to trip circuit breaker CB2.

Table 3.2 and Table 3.3 show the thresholds on both voltage and frequency parameters respectively, according to the IEEE Std. 1547-2003 and IEEE Std. 929-2000 [7].

Table 3.2: System response to abnormal voltage operations.

| Voltage at PCC | Maximum Trip time |
|---|---|
| V< 50 % | 6 cycles |
| 50 %< V < 88 % | 120 cycles |
| 88 %< V < 110 % | Normal Operation |
| 110 %< V < 120 % | 60 cycles |
| V > 120 % | 6 cycles |

Table 3.3: System response to abnormal frequency operations.

| Voltage at PCC | Maximum Trip time (sec) |
|---|---|
| f > 60.5 | 0.16 |
| f < 59.3 | 0.16 |

Before testing the UOF/UOV performance on the simulated model, the relationship between the power mismatch thresholds and the voltage/frequency

thresholds was found analytically to be as shown in equations (3.9) and (3.10) [21]. The detailed derivation of equations (3.9) and (3.10) is found in APPENDIX B.

$$\left(\frac{V}{V_{max}}\right)^2 - 1 \leq \frac{\Delta P}{P} \leq \left(\frac{V}{V_{min}}\right)^2 - 1 \tag{3.9}$$

$$Q_f.\left(1 - \left(\frac{f}{f_{min}}\right)^2\right) \leq \frac{\Delta Q}{P} \leq Q_f.\left(1 - \left(\frac{f}{f_{max}}\right)^2\right) \tag{3.10}$$

Where: $V_{max}$; $V_{min}$; $f_{max}$ and $f_{min}$ are the UOV/UOF thresholds. Typically, $V_{max} = 110\%$, and $V_{min} = 88\%$ of the nominal voltage. $f_{max} = 60.5Hz$ and $f_{min} = 59.3\ Hz$ . Then for $Q_f = 2.5$:

$$-17.36\% \leq \frac{\Delta P}{P} \leq 29.13\% \tag{3.11}$$

$$-5.94\% \leq \frac{\Delta Q}{P} \leq 4.11\% \tag{3.12}$$

The results show that if the power and reactive power mismatch are within the calculated thresholds then the voltage and frequency of the system will remain within the acceptable limits even if an island is formed. As a result, any island maybe formed and sustain without being detected. Equations (3.11) and (3.12) may form an area which is called the Non detective zone (NDZ), as shown in Figure 3.8.

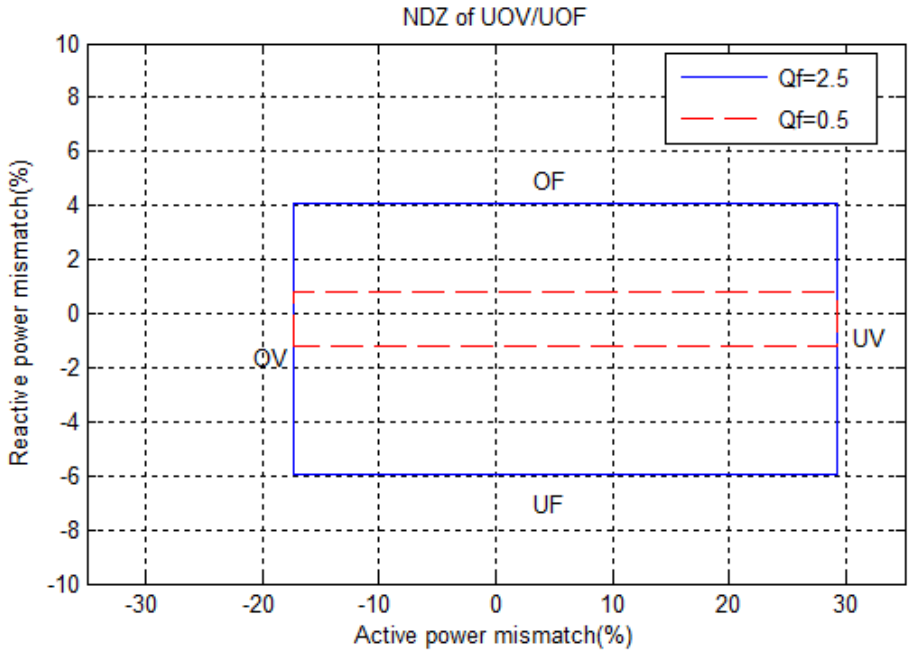


Figure 3.8: NDZ of UOV/UOF with different quality factors.

The analytical results are then validated by PSCAD simulation of the system model explained in section 3.1. The NDZ of the simulation for quality factor = 2.5 is mapped in Figure 3.9.

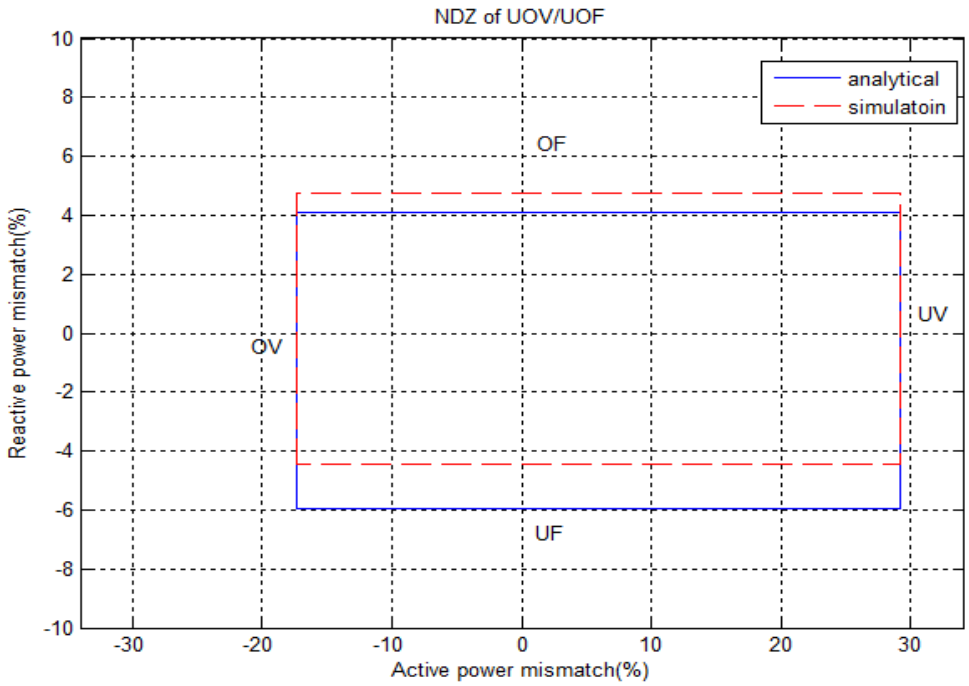


Figure 3.9: Analytical and simulation NDZ of UOV/UOF when quality factor = 2.5.

It is noted from Figure 3.9 that some differences between the analytical and the simulation result exist. These differences are due to the omission of quadratic terms in the analytical derivation found in Appendix A [21].

The following few points can be concluded from equations (3.11), (3.12), and Figure 3.8 :

- UOF/UOV passive techniques have a large NDZ for this specific inverter's control.
- Reactive power mismatch is more sensitive than active power mismatch.
- UOV non-detective zone is dominant by the active power mismatch, while UOF non-detective zone is dominant by the reactive power mismatch.
- It is evident from Figure 3.8 that as the quality factor increases the NDZ increases. Since the higher the quality factor is the stronger the resonance. In this case it will be difficult to drift the frequency of the power island.

Figure 3.10 shows an islanding event took place at t = 0.3sec. The power mismatch is within the NDZ ($\Delta P = \Delta Q = 0$). It is evident from Figure 3.10 that the passive technique failed to detect the islanding. On the other hand Figure3.11 shows the same case with power mismatch ($\Delta Q = 4.33\%$). It is clear from Figure 3.11 that the islanding is detected since the system frequency deviated beyond the acceptable limits, this deviation is due to the reactive power mismatch.

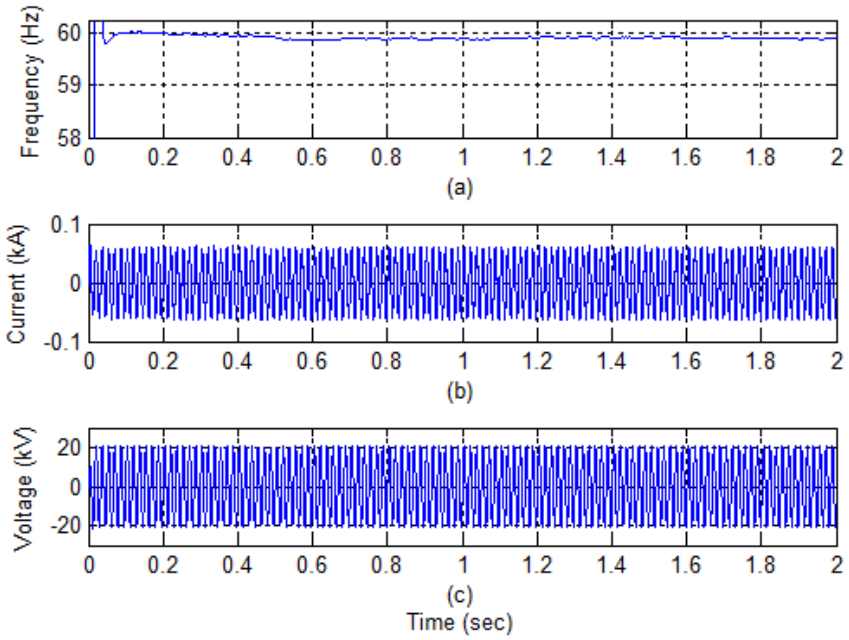


Figure 3.10: Simulation result for system (a) frequency (b) current (c) Voltage when the power mismatch is within the NDZ.

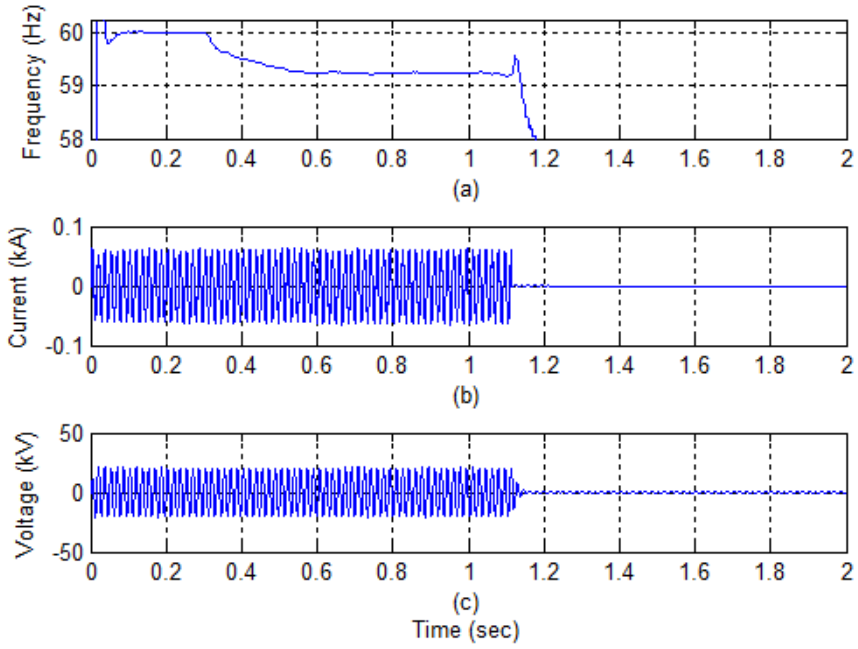


Figure 3.11: Simulation result for system (a) frequency (b) current (c) Voltage when ($\Delta P = 0\%, \Delta Q$=4.33%).

## 3.3 Detection of Harmonics' Principle of Operation and Simulation Results

In this method, the inverter controller will monitor the THD of the inverter's voltage at PCC as explained in section 3.1.5 and will send a trip signal to disconnect the DG if the THD exceeds a threshold. During the grid connected mode, low THD is maintained at the PCC. This is because the utility generally have low impedance. So the harmonic current interacting with low impedance will produce a small amount of distortion in the PCC voltage. However, when the grid is disconnected and an island is formed, the harmonic currents produced by the inverter will flow into the load, which in general has much higher impedance than the utility leading to a larger harmonics in PCC voltage. This change in voltage harmonics can be monitored in order to decide the occurrence of an islanding event. Moreover, the presence of non-linear loads in the power island (i.e. the distribution step down transformer) will be excited by the output current of the inverter. Hence, the voltage response to the current excitation can be highly distorted [7].

DH promises to be highly successful in islanding detection. However, DH method suffers from the problem of selecting the appropriate threshold. The threshold selected should be a) higher than the THD produced during grid connected mode; b) lower than the THD produced during islanding situations. Hence, it is difficult to set a threshold that will detect islanding and at the same time does not cause false tripping[12]. Figure 3.12 shows the percentage of THD calculated for the three phases of the voltage signal at the PCC when islanding took place at t =0.3 sec. The load has a quality factor of 2.5 and reactive power mismatch equal to 5%. If the threshold was selected to be 5% which is the maximum allowable THD set by the power quality standards then the islanding event will be detected since the THD exceeds the preset threshold. Figure 3.13 shows the percentage of THD when a capacitor bank is switched at t = 0.3sec. It is observed from Figure 3.13 that the percentage exceeded 5% though an islanding has not taken place. Thus, transient voltage disturbances especially large ones such as switching of a capacitor bank as shown could lead to an increase in THD which might be falsely interpreted as islanding event. It is clear that it is not possible to select a threshold that meets criteria a) and b).

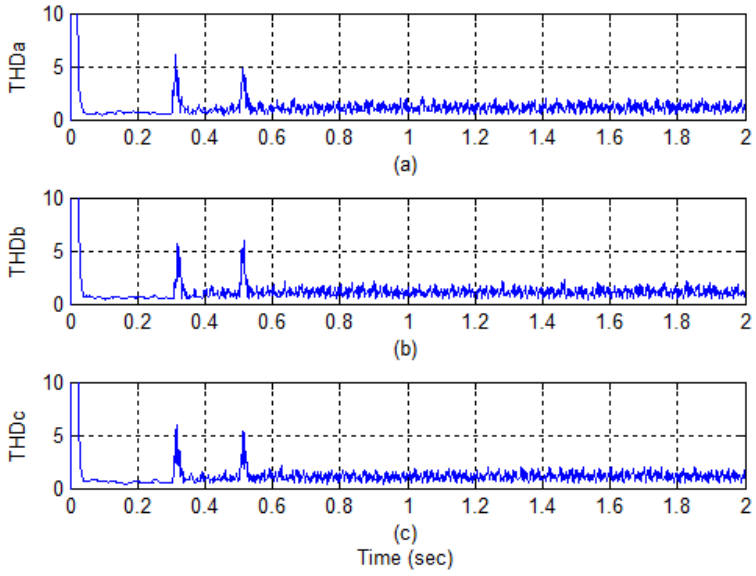


Figure 3.12: Percentage of THD calculated for (a) phase a (b) phase b and (c) phase c when islanding took place at t = 0.3sec ($\Delta P = 0\%, \Delta Q = 5\%$ , $Q_f = 2.5$).

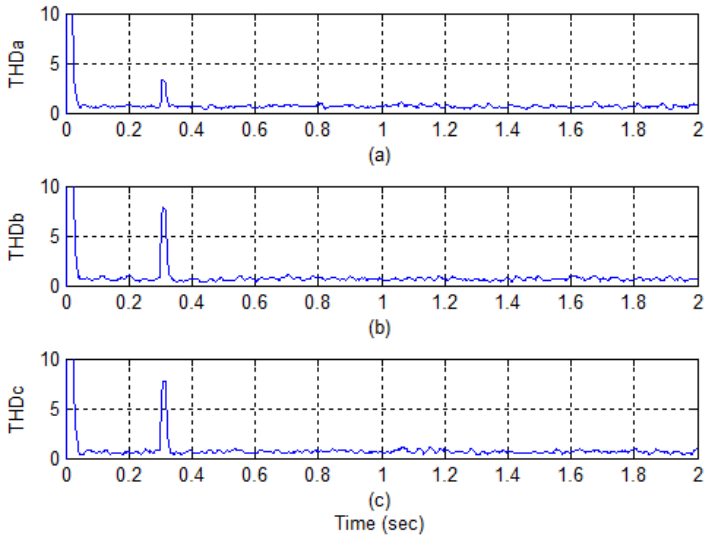


Figure 3.13: Percentage of THD calculated for (a) phase a (b) phase b and (c) phase c when switching of capacitor bank took place at t = 0.3sec.

Figure 3.14 shows an islanding event took place at t = 0.3sec under power balanced conditions ($\Delta P = \Delta Q = 0$) and a load of 2.5 quality factor. It is evident the passive technique failed to detect the islanding. The failure is due to the high quality factor of the parallel RLC load which attenuates the higher frequency components and exhibits low pass filter characteristics. On the other hand, Figure 3.15 describes the

same case but with a load having quality factor of 0.5. It is clear that the THD percentage is greater than the previous case (load with 2.5 quality factor) yet the islanding has not been detected when a threshold of 5% was chosen. Since the parallel RLC load can exhibits low pass characteristics that attenuate higher frequency components it is more convenient to set a threshold lower than 5%.

The results suggest that THD is not always capable of detecting islanding. The method is affected by transient voltage disturbance, quality factor of loads, and the presence of power electronics devices which produce current harmonics. Hence, DH suffers from nuisance tripping.

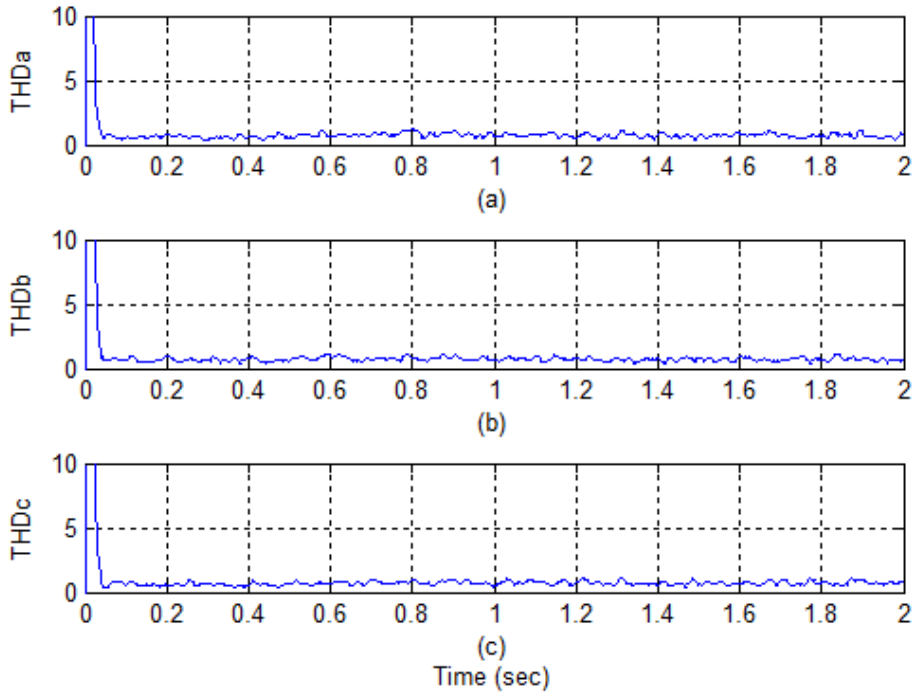


Figure 3.14: Percentage of THD calculated for (a) phase a (b) phase b and (c) phase c when islanding took place at t = 0.3sec ($\Delta Q=\Delta p = 0$ % , $Q_f = 2.5$).

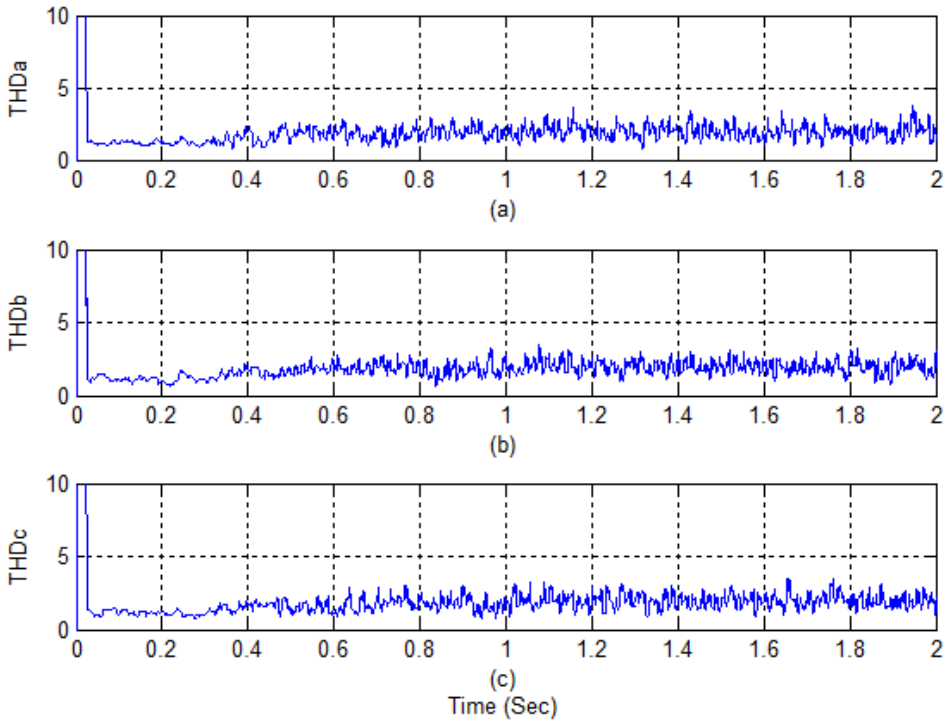


Figure 3.15: : Percentage of THD calculated for (a) phase a (b) phase b and (c) phase c when islanding took place at t = 0.3sec ($\Delta Q = \Delta p = 0\%$ , $Q_f = 0.5$).

## 3.4 Summary

The chapter identified the limitations of UOF/UOV and DH passive techniques. UOF/UOV islanding techniques have large NDZ and fail to detect islanding in case of power match in the power island especially with high quality factor load. When using the DH method it is difficult to select an appropriate threshold that provide islanding detection and at the same time do not lead to false tripping. Therefore, these techniques have limitations and they should be combined with other islanding detections techniques especially in the presence of multiple DGs in the distribution network.

# CHAPTER 4

# PROPOSED ISLANDING DETECTION TECHNIQUE

The proposed technique is based on the identification of the transients associated with islanding, and differentiating them from the transients associated with non-islanding events such as faults, switching.

In this chapter, the proposed Neuro-wavelet based islanding detection technique is explained. The chapter starts with an overview of artificial neural networks (ANN) followed by an explanation of the training process. Section two gives a brief introduction to wavelet transform including its theory, choice of mother wavelet, and practical implementation of wavelets. Section three presents the methodology of the proposed Neuro-wavelet technique. Finally, results and discussion are given in section 4 and 5, respectively.

## 4.1 Artificial Neural Networks

Artificial neural networks (ANNs) have been used in many potential applications in power systems operation and control. Load forecasting, fault diagnosis/fault location, economic dispatch, transient stability and harmonics analysis are some of the application in which ANN was adopted as a classifier [23]. ANNs are often used as classifiers since they have the capability of learning complex mapping, linear or nonlinear from the input space to the output space [24]. The architecture and the training algorithm of the feed forward artificial neural network are described in the following sections.

### 4.1.1 Artificial Neural Network Architecture

ANN consists of simple processing units, called neurons, operating in parallel to solve specific problems. Figure 4.1 shows a simple neuron with input vector **P** of dimension $R \times 1$ . The input **P** is multiplied by a weight **W** of dimension$1 \times R$. Then a bias $b$ is added to the product **WP**. $f$ is a transfer function (called also the activation function) that takes the argument $n$ and produces the net output a. The most commonly used transfer functions are shown in Figure 4.2. Both the weight and the bias are adjustable parameters of the neurons.

The idea of ANN is that these parameters ($w \; and \; p$) are adjusted so that the network exhibits some desired behavior. Thus the network can be trained to do a particular job by adjusting the weight or bias parameters [25].

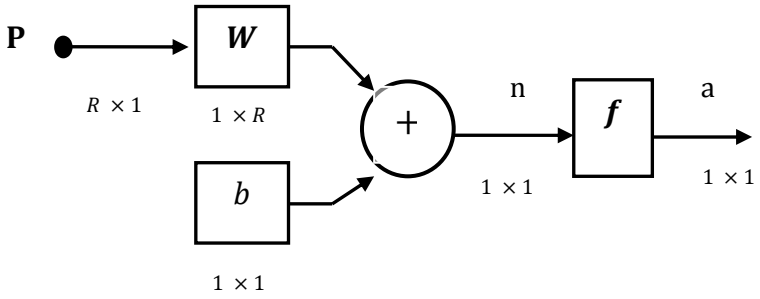


$$a = f(\mathbf{WP} + b)$$

Figure 4.1: Neuron.

A neuron with a hard-limit activation function is called a perceptron and it is used for classification purposes. Since, the hard-limit activation function divides the input space into two regions. The perceptron produces 1.0 if the net output is greater or equal to 0, otherwise it produces a 0. On the other hand, a neuron with purelin activation function is used for linear approximation purposes. The linear (purelin) and sigmoid (tansig, logsig) activation functions are used in backpropagation networks which will be explained later in this section since they are differentiable [24].

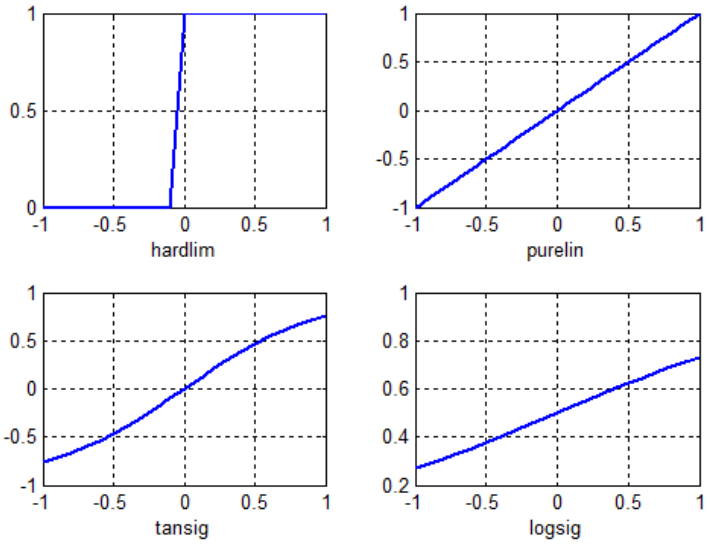


Figure 4.2: Transfer functions.

A number of neurons can be combined together to form a layer of neurons. A one layer of $R$ input elements and $S$ neurons is shown in Figure 4.3 [24].

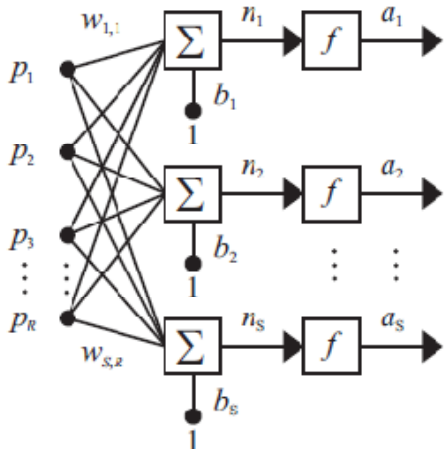


Figure 4.3: One layer network of $R$ input elements and $S$ neurons.

A network can have many layers of neurons to form multiple layers of neurons. Figure 4.4 illustrates three layers of $R$ input elements and $S$ neurons. The layer that produces the network output is called an output layer. All other layers are called hidden layers. The three layer network is shown in Figure 4.4 has one output layer and two hidden layers [24].

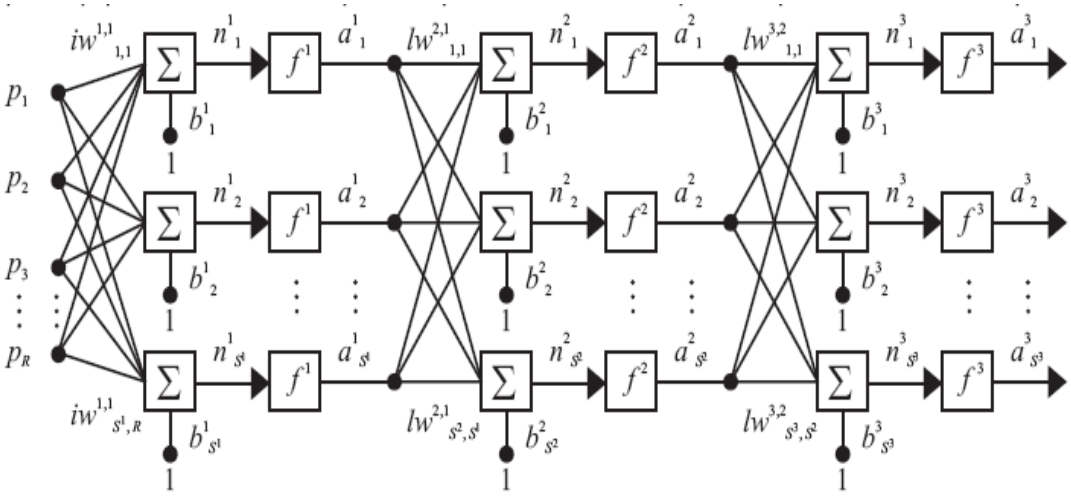

Figure 4.4: Three layer network of $R$ input elements and $S$ neurons.

### 4.1.2 Training the ANN

A *training algorithm* is defined as a procedure of updating the weights and biases of a network so the network will be able to perform the particular design task. The training algorithm is divided into two main categorizes: supervised learning, and unsupervised learning. ANN is classified under supervised learning. In the training stage, the training data set and the corresponding targets are entered to the model. Once the network weights and biases are initialized, the network is ready for training. The weights and biases are then adjusted in order to minimize the mean square error MSE (the average squared error between the networks outputs $a$ and the target outputs $t$). This can be achieved using the gradient of the MSE.

The gradient descent algorithm is determined using a technique called *backpropagation* [24]. The steps of converging to the optimal solution can be summarized as follows:

1. The network first uses the input vector to produce its output vector.
2. The difference between the obtained target value and the actual target will be computed. This is referred to as the prediction error.
3. The error will propagate backward through the network and the gradient (derivatives) of the change in error with respect to changes in weight values will be computed.

4. The weights will be updated accordingly to reduce the error.

Each cycle is called an epoch.

There are several issues involved when training multiple layers NN:

- Selecting the number of hidden layer

  Network with one hidden layer is sufficient for solving most of the problems [24]. Though having more than 1 hidden layer for some application may result in faster learning. However networks with more than one hidden layer will increase the probability of converging to local minima.

- Deciding the number of Neurons in the hidden layers

  If a small number of neurons are used, the network will be unable to model complex data, and the resulting fit will be poor. On the other hand, if too many neurons are used, the training time may become long and the network may over fit the data. When overfitting occurs the result is that the model fits the training data extremely well, but it generalizes poorly to novel data. The number of neurons chosen should correspond to the best performance on the validation data.

## 4.2 Wavelet Transform

Real time transients classification of power transients is very challenging since the high frequency content superimposed on the power frequency signals are usually aperiodic, short term and non stationary waveforms. Wavelet transform is proposed in order to extract discriminative features which will help in differentiating between transients associated with islanding event and those created from any other event such as switching of capacitor bank and temporary fault.

Wavelet transform (WT) is an effective mathematical tool which has been widely used in many engineering applications such as speech and image processing. WT has found many numerous applications in the power systems field some of the applications are power system protection, power quality, and partial discharge.

Unlike Fourier transform (FT) which transforms the signal from the time domain to the frequency domain. The WT extract the frequency components of the signal while preserving the time domain properties [26]. The theory of WT will be explained in the following section.

### 4.2.1 Theory of Wavelet Transform

Traditionally, the FT has been used extensively in signal processing to analyze stationary or time-invariant signals. In FT the analyzed signal is decomposed into a combination of sinusoidal waves having different frequencies. The FT is defined in (4. 1).

$$X(f) = \int_{-\infty}^{\infty} x(t)e^{-j2\pi ft}dt \tag{4.1}$$

Equation (4.1) defines the Fourier transform $X(f)$ at the specific frequency $f$ to be the time integral over all time of the product of a given signal $x(t)$ with a complex sinusoid at the specified frequency $f$.If the signal has a strong component at the particular frequency $f$, the FT will be significant. Otherwise it will be negligible. Since FT is the sum of the coefficient all over time, the coefficient does not give an indication of the time at which a certain frequency exists. Thus, FT provides perfect frequency resolution but no time resolution. In order to overcome the deficiency of FT, a short-time Fourier Transform (STFT) was developed. In STFT the analyzed signal is segmented or windowed using a chosen window. STFT will map the analyzed signal into both time and frequency domain. In other words, STFT computes the FT on the segmented portion of the analyzed signal. If the window size chosen is large then, a larger portion of the segmented signal is considered resulting in good frequency resolution but poor time resolution. On the contrary, if the window size chosen is small, then a smaller portion of the segmented signal will be considered resulting in good time resolution but poor frequency resolution. STFT compromise between time and frequency information could be useful depending on the application. However, once the time window size is chosen it will be fixed for all frequencies. Many signals require a more flexible approach where the window size could be varied to determine more accurately either time or frequency. WT analysis represents the next logical step: a windowing technique with variable-sized regions. WT analysis allows the use of long time window intervals where more precise low-frequency information is needed, and

shorter regions where high-frequency information is desired. Hence, Wavelet analysis is capable of providing time localization of the analyzed signal.

Similar to FT which breaks the signal into sinusoidal waves of different frequencies; WT breaks the signal into shifted and dilated version of a short term waveform called mother wavelet. Mathematically, the continuous wavelet transform (CWT) of a signal can be represented by:

$$CWT_x^{(\varphi)}(a,b) = \frac{1}{\sqrt{a}}\int_{-\infty}^{\infty} x(t).\varphi^*(\frac{t-b}{a})dt \qquad (4.2)$$

Where: $a$ is the scale, $b$ is the translation or position, $x(t)$is the analyzed signal, and $\varphi$ is the mother wavelet described in (4. 3).

$$\varphi_{a,b}(t) = \frac{1}{\sqrt{a}}\,\varphi\left(\frac{t-b}{a}\right) \qquad (4.3)$$

The definition of CWT shows that the wavelet analysis is a measure of the resemblance between the wavelet and the original signal. The calculated coefficient refers to the correlation or similarity between the function and the wavelet at the current scale. If the coefficient is relatively large then the signal is similar to the wavelet at this point in time-scale plane. In practical implementation of CWT there will be redundant information. Therefore, for the ease of computational purposes the scale and translation variables are discretized. The discrete wavelet transform is described in (4. 4).

$$DWT_\varphi\ f(m,n) = \sum_k f(k)\,\varphi^*_{m,n}(k) \qquad (4.4)$$

Where, $\varphi_{m,n}$ is the discretized mother wavelet given by (4. 5):

$$\varphi_{m,n}(t) = \frac{1}{\sqrt{{a_0}^m}}\,\varphi\left(\frac{t-b_0{a_0}^m}{{a_0}^m}\right) \qquad (4.5)$$

Where $a_o > 1$ and $b_o > 0$ are fixed real values, $m$ is the scale and $n$ is the translation are positive integers.

### 4.2.2 Choice of mother wavelet

In wavelets applications, the choice of appropriate mother wavelet plays an important role in the analysis. Different basis functions have been proposed. These include Haar, Morlet, Mexican, Daubechies, etc. The choice of mother wavelet depends on the application. For example in signal processing in real time, computation efficiency may be of importance to be considered. For classification of power quality disturbance signals, the choice revolves of discrimination between various transients [26].

Daubechies wavelet family is one of the most suitable wavelet families in analyzing power system transients as investigated in [9], [19], and [26]. In the present work, the db1 wavelet shown in Figure 4.5 (with two filter coefficients) has been used as the mother wavelet for analyzing the transients associated with islanding. db1 is a short wavelet and therefore it can efficiently detect transients.

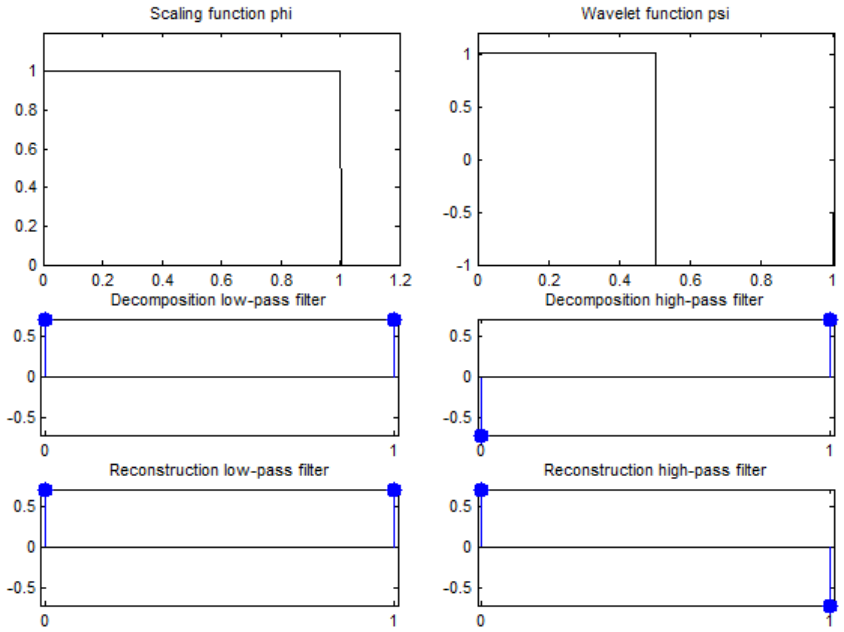


Figure 4.5: db1 mother wavelet.

### 4.2.3 Discrete wavelet transform's practical implementation

The WT can be implemented with a specially designed pair of FIR filters called a quadrature mirror filters (QMFs) pair. The discrete wavelet transform (DWT) is computed by successive low pass and high pass filters which are combined in a tree structure. The filter bank is able to decompose the signal into low and high frequency components. These filters are combined with down sampling operators which will de-sample the signal by a factor of two [27].

Implementation of three levels WT is illustrated in Figure 4.6 . In order to get the DWT of a signal S, The original signal S is passed through a low pass filter LP and high pass filter HP. The resulting signal from LP is a smoothed version of the original signal S and called the approximation signal (A1). While, the resulting signal from HP is a detailed signal of the original signal S and called the detail signal (D1). D1 is the WT coefficient at level one. Similarly, D2 is the WT coefficient at level two.

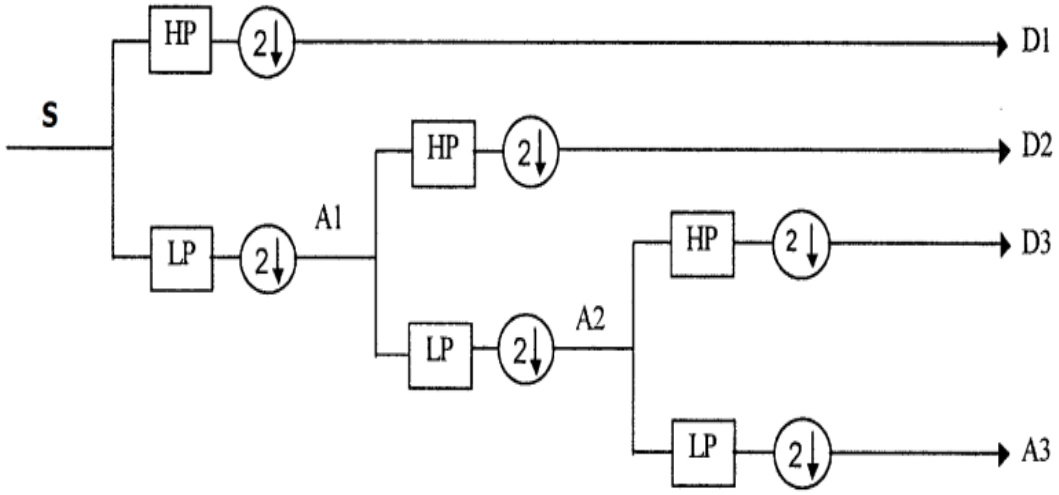


Figure 4.6: Implementation of three levels WT.

## 4.3 Methodology

The proposed method utilizes and combines wavelet analysis and artificial neural network. Wavelet transform is capable of decomposing the signals into different frequency bands. It can be utilized in extracting discriminative features from the acquired voltage signals. The features are then fed to a trained ANN model which if well trained is capable of detecting islanding and differentiating between islanding events and any other events that have transients such as switching or temporary fault.

In the proposed technique, prescribed events are simulated. The voltage signals at the DG side are acquired in order to be analyzed using WT. The discriminative features are then captured and fed to a trained ANN model. The ANN considered two classes namely: non-islanding and islanding. A general block diagram of the proposed method is illustrated in Figure 4.7.

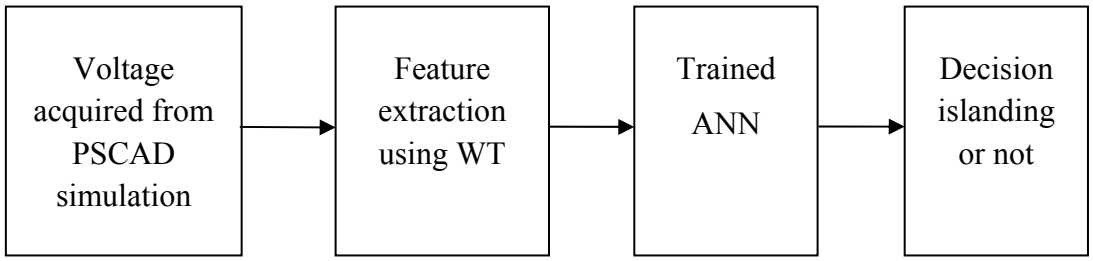


Figure 4.7: General methodology block diagram.

The system under study is simulated in PSCAD as discussed in chapter three. The system model contains three DGs. The simulated DGs are inverter based PV panel identical to each other i.e. they have the same DC input and current controller scheme. The system model with three DGs is shown in Figure 4.8. Adding multiple DGs connected to the same point of common coupling will affect the islanding detection technique due to the interferences between the sources [28].Moreover, the possibility of the islanding detection technique to malfunction is higher when having multiple DGs than having single DG. This is because the total amount of the output power of each DG can change to match the load connected to the line [29].

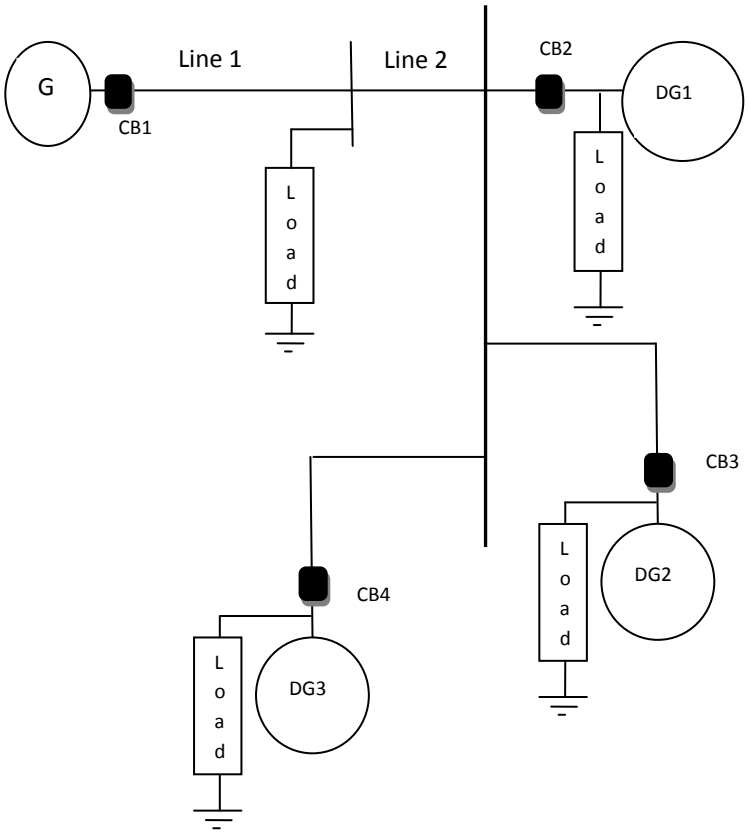


Figure 4.8: System model with three DGs.

Two different sets of data which correspond to the two different classes (islanding and non-islanding) are simulated in PSCAD. The simulated non-islanding cases include adding and removing of different loads, adding and removing of capacitor banks, and temporary single line to ground (SLG), line to line to ground (LLG), and three phases to ground faults at different inception angles and at different locations of the distribution network. Furthermore, the events simulated under the following states:

- Different utility grid operating states, including normal system loading, and different system loading.
- Different DG operating states, including normal DG loading, and different DG loading.

On the other hand, the islanding cases simulated include opening of circuit breakers CB1, CB2, CB3 or CB4, shown in Figure 4.8, at different times within one cycle in case of matched and unmatched power.

Voltage signals for the different mentioned cases are then acquired from the DG PCC. WT will be carried out on the obtained voltage signals to extract the features. The purpose of feature extraction is to identify specific signature of the voltage waveforms that can detect islanding and differentiate between islanding and any other transient condition.

A transient signal can be fully decomposed into smoothed signals and detailed signals for *L* wavelet levels. In wavelets applications, Daubechies wavelet family is one of the most suitable wavelet families in analyzing power system transients as investigated in [9], [19], and [26]. In the present work, db1 wavelet has been used as the mother wavelet for extracting the energy content of the detail coefficient of voltage waveforms. db1 is a short wavelet and therefore it can efficiently detect transients. The voltage signals were decomposed for 7 wavelet levels. Table 4.1 gives the frequency band information of the wavelet analysis. The sampling frequency is 10 kHz. Details (D1- D7) were used for feature extraction. Other details are ignored due to the low frequency components which is below the fundamental frequency 60 Hz.

Table 4.1: Frequency band information for the different levels of wavelet analysis.

| Wavelet level | Frequency Band (Hz) | Wavelet level | Frequency Band (Hz) |
|---|---|---|---|
| 1 – D1 | 2500-5000 | 5 – D5 | 156.25-312.5 |
| 2 – D2 | 1250-2500 | 6 – D6 | 78.125-156.25 |
| 3 – D3 | 625-1250 | 7 – D7 | 39.0625-78.0625 |
| 4 – D4 | 312.5-625 | A7 | 19.5-39.025 |

The energy content in the details of each decomposition level for all voltage signals was calculated using the detail coefficients in the corresponding level. Equation (4. 6) shows the calculation of the energy content for the first detail (D1). The energy content in the other decomposition levels can be calculated the same way.

$$\|ED_{1a}\| = \left[\sum_{k} d_k^2\right]^{\frac{1}{2}} \tag{4.6}$$

Where: $ED_{1a}$ is the energy content of D1 for voltage signal of phase (a) and $d_k$ is the *kth* coefficient in the first decomposition level.

The energy content determined using (4.6) is extracted from the details in each of the three-phase voltage signals. The feature vector chosen corresponds to the summation of energies for phases a, b, and c. Figure 4.9 illustrates the features extracted from the voltage signal in phase a.

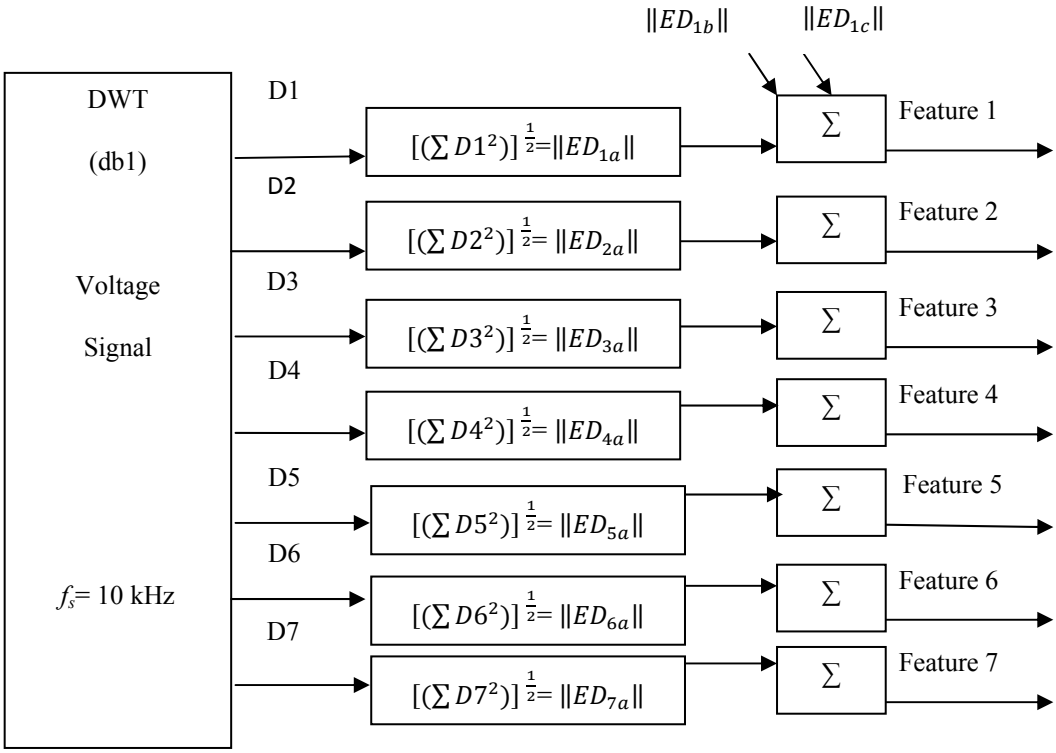


Figure 4.9: Feature extraction methodology.

After collecting the features for the simulated different cases, the features will be fed to a trained ANN in order to identify whether the event took place is islanding or non-islanding event. Figure 4.10 shows a detailed flow chart of the proposed algorithm.

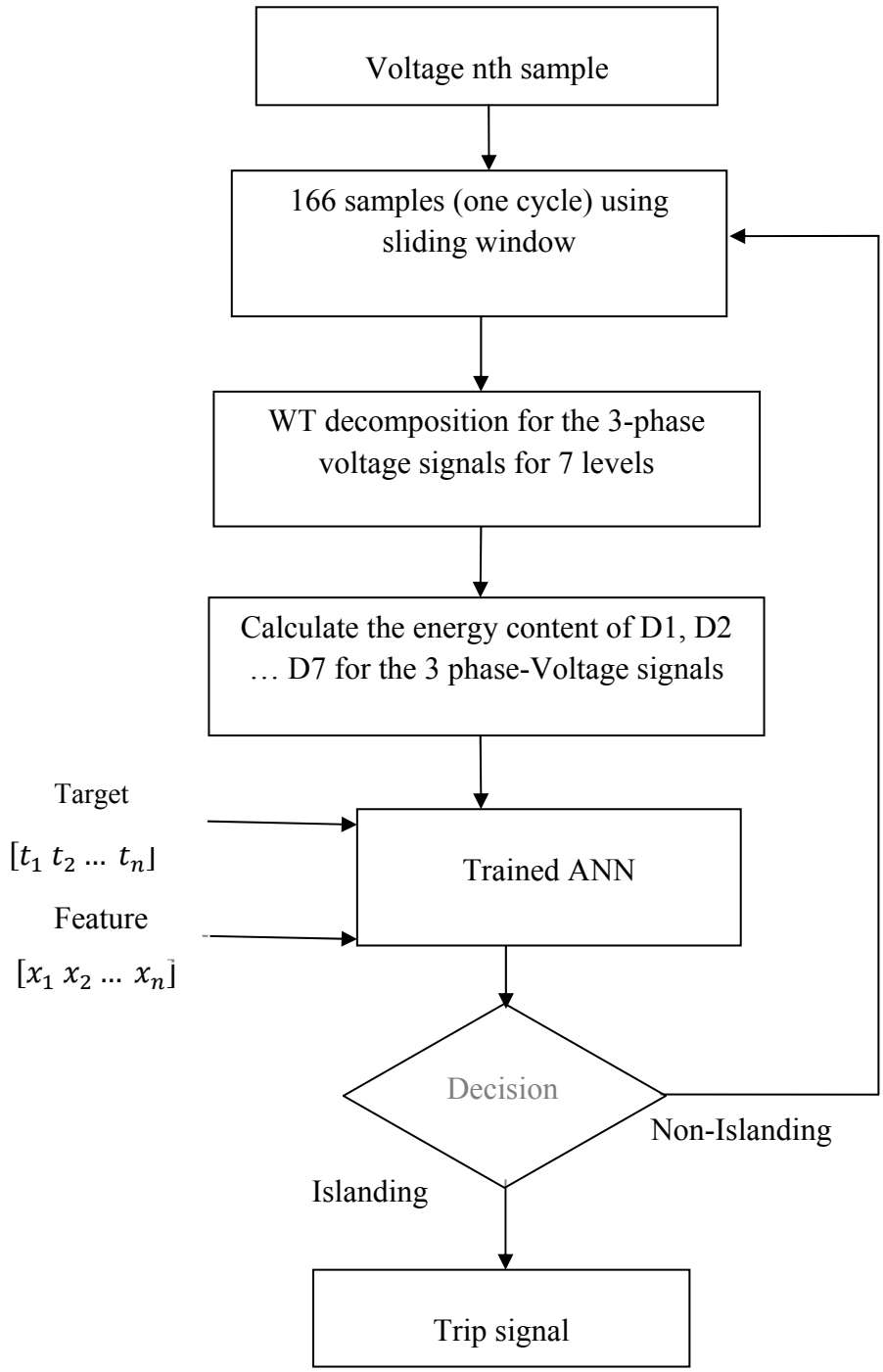


Figure 4.10: Flow chart of the proposed algorithm.

The algorithm starts by collecting a one cycle sampled data window for each signal. Based on a sampling frequency of 10 kHz, one cycle contains 166 samples. A sliding data window of 0.0166 seconds is used. DWT will be then carried out and the energy content of the wavelet details for the acquired voltage waveforms will be

calculated. The feature vector will be then fed to a trained ANN. A decision whether or not an islanding has took place will be taken with the help of the trained ANN.

## 4.4 Results

The proposed method explained in section 4.3 is applied on the testing circuit discussed in chapter three. Figures 4.11-4.17 illustrate an example of the wavelet details (D1-D7) of 2 cycles voltage waveform acquired from phase (a) at DG1 when four different events have took place. These events have taken place at time = 0.016sec. It is evident from Figures 4.11 -4.17 that some differences exist in the different types of events can be noticed by the naked eye. Figures 4.11-4.17 consist of four different graphs. The first graph shows an islanding event when the power generated from the DG match the power consumed by the load. On the other hand, the second graph demonstrates an islanding event in case of power mismatch. It can be noticed from the graph that the transients generated when there is power mismatch is more than the transients generated when power match. Thus, it is easy to detect islanding when power mismatch using simple passive technique as discussed in chapter three. The third graph represents a switching of load event near the DG. Three-phase-to-ground fault event is shown in the last graph. It is noticed from the graphs that during the fault the details dropped to zero since the DG is equipped with UOF/UOV protective relay which isolated the fault.

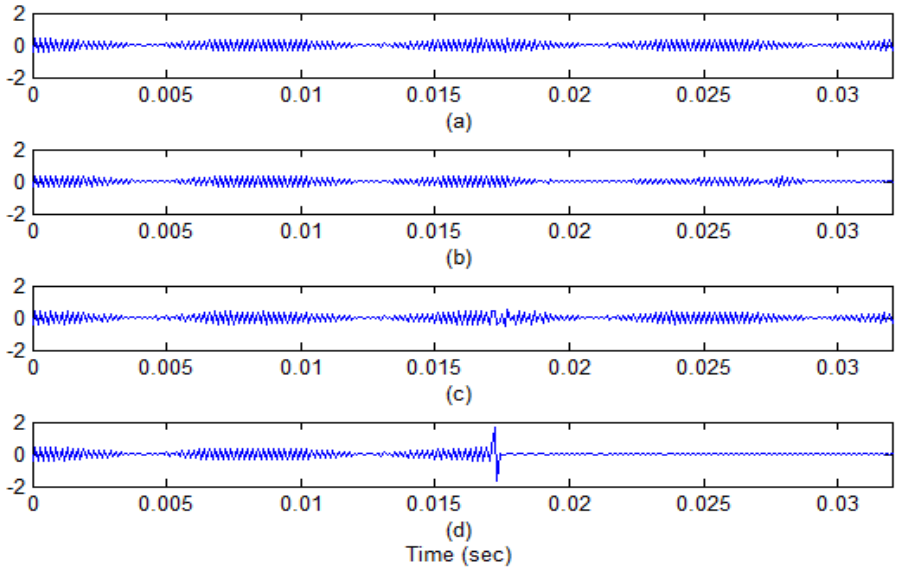


Figure 4.11: Wavelet detail d_1 of voltage waveform in case of (a) islanding when power match, (b) islanding when power mismatch, (c) switching of load, and (d) three-phase-to-ground fault.

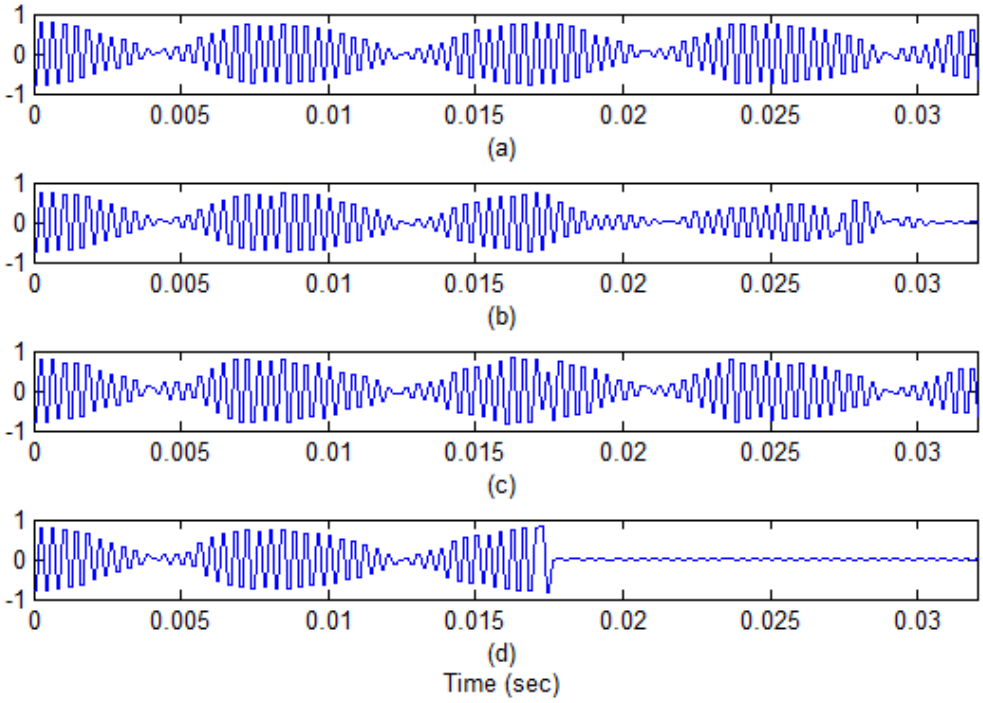


Figure 4.12: Wavelet detail d_2 of voltage waveform in case of (a) islanding when power match, (b) islanding when power mismatch, (c) switching of load, and (d) three-phase-to-ground fault.

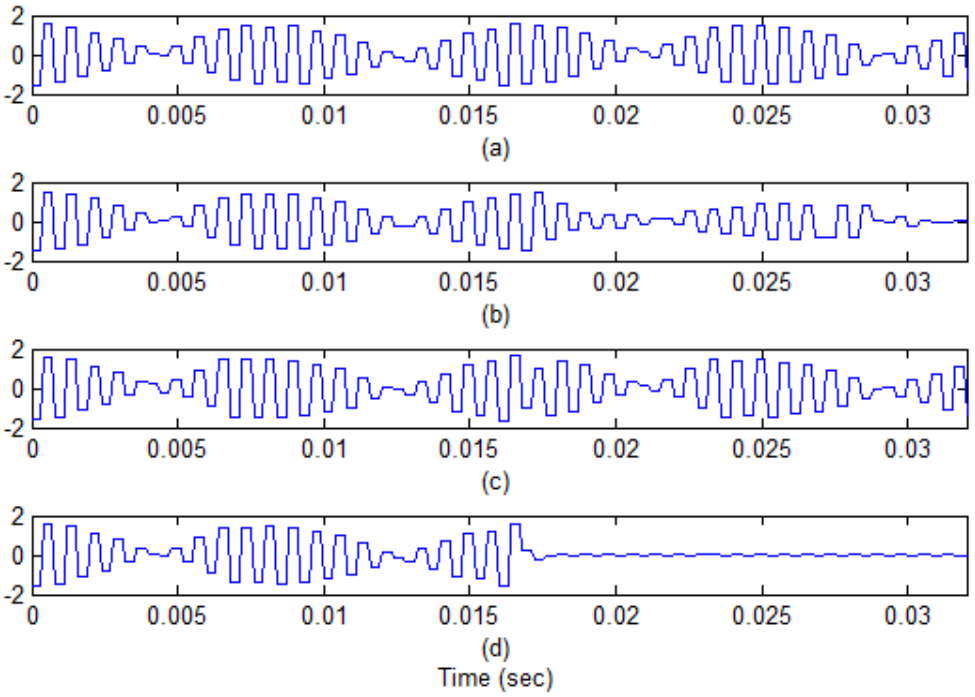


Figure 4.13: Wavelet detail d_3 of voltage waveform in case of (a) islanding when power match, (b) islanding when power mismatch, (c) switching of load, and (d) three-phase-to-ground fault.

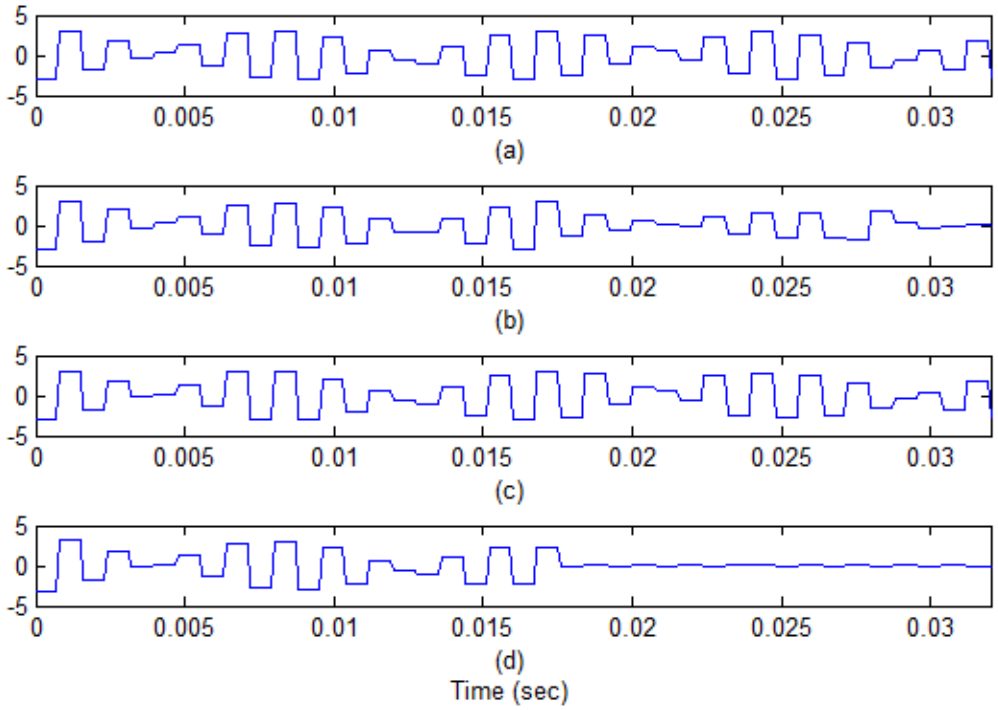


Figure 4.14: Wavelet detail d_4 of voltage waveform in case of (a) islanding when power match, (b) islanding when power mismatch, (c) switching of load, and (d) three-phase-to-ground fault.

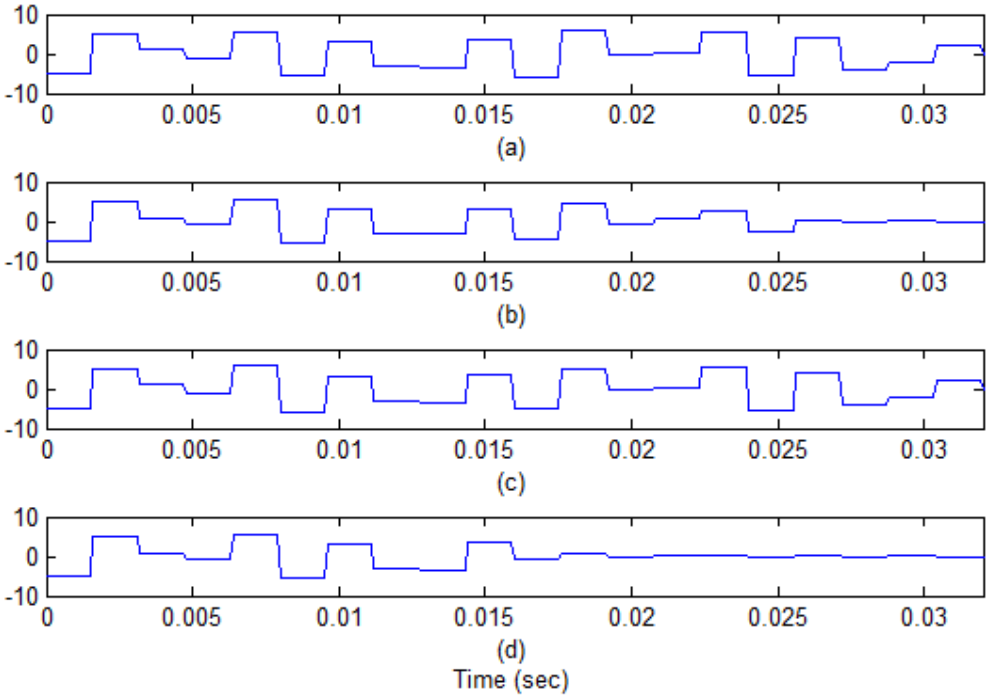


Figure 4.15: Wavelet detail d_5 of voltage waveform in case of (a) islanding when power match, (b) islanding when power mismatch, (c) switching of load, and (d) three-phase-to- ground fault.

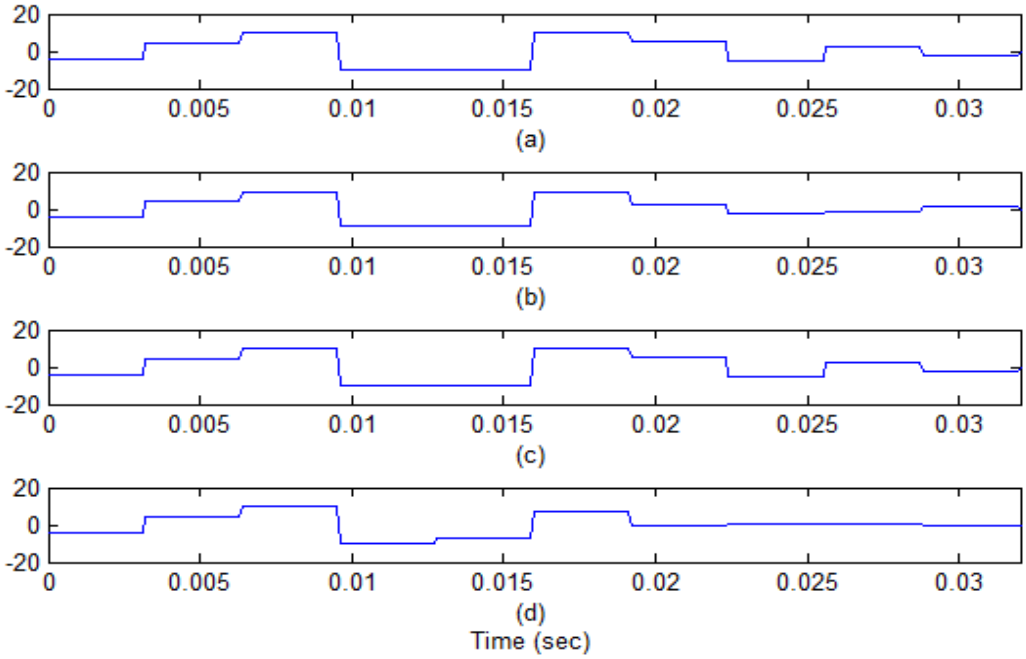


Figure 4.16: Wavelet detail d_6 of voltage waveform in case of (a) islanding when power match, (b) islanding when power mismatch, (c) switching of load, and (d) three-phase-to- ground fault.

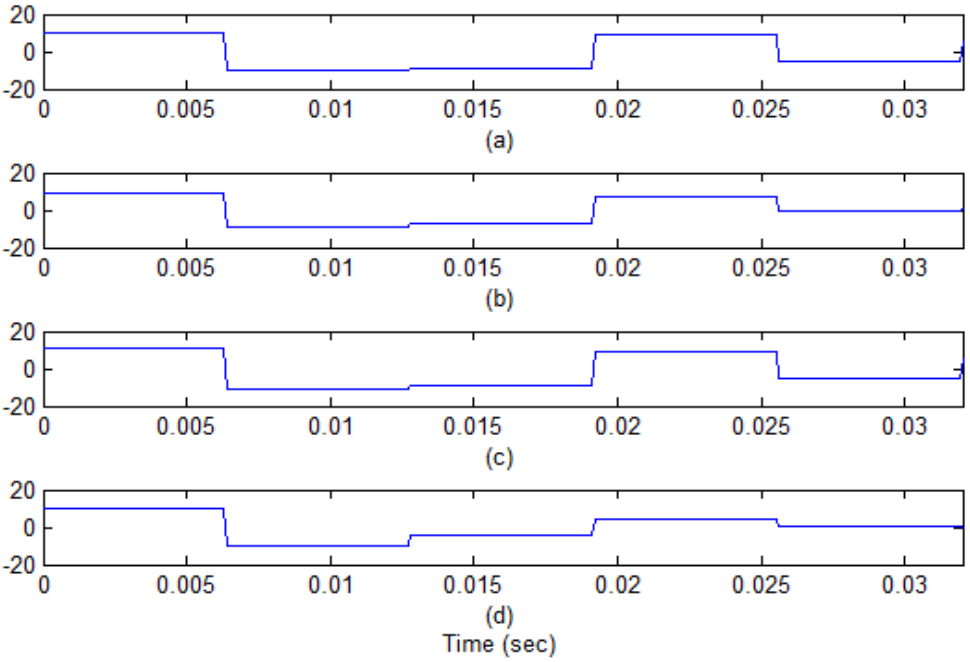


Figure 4.17: Wavelet detail d_7 of voltage waveform in case of (a) islanding when power match, (b) islanding when power mismatch, (c) switching of load, and (d) three-phase-to- ground fault.

It is evident from Figures 4.11-4.17 that some differences can be noticed between the four different events when analyzing the voltage waveforms using DWT. This variation in the waveform patterns lead to a different energy distribution from one event to another. However, one certain threshold does not discriminate between the different clusters. Hence, an artificial intelligence technique using artificial neural network (ANN) was adopted. ANN is often used as a classifier since it has the capability of learning complex mapping, linear or nonlinear from the input space to the output space as explained in section 4.1.

A total of 540 islanding and non-islanding cases for DG1, DG2 and DG3 were simulated. Three distinctive training sets of 120 simulated cases and testing sets of 60 cases were used to train and validate each model.

In order to generalize the ability of the ANN classifier, cross- validation technique is used. In cross-validation, the available simulated data are divided into *k* disjoint sets, *k* models will be trained and tested using different combinations of the portioned data. The performance is then determined using the mean of the performance evaluated for each of the *k* models over the corresponding test partitions of the data [9]. In this work, 3-fold cross-validation was carried out. The database will be partitioned into 3 different subsets. Of the three subsets, two subsets are used for training the model and the remaining subset is used for testing the model. Then the same process is repeated 3 times until the whole data sets are used for testing the model. Three different models for the same DG will be then generated out of three different combinations of the total 180 data.

The performance of ANN for DG1, DG2 and DG3 of the first fold are shown in Tables 4.2-4.10. The accuracies obtained in Tables 4.2-4.10 represent the performance of the proposed technique when power match ($P_{dg} = P_{load}$ and $Q_{dg} = Q_{load}$) which correspond to the worst case for passive anti-islanding detection methods as discussed in chapter three. Moreover, the performance of the method is tested in case of power mismatch and islanding is detected successfully.

Table 4.2: Performance matrix of DG1 (fold1).

| Fold (1) | | Islanding | Non-islanding | | | |
|---|---|---|---|---|---|---|
| | | Matched | Switching of load | Switching of Capacitor bank | Faults | Normal operation |
| Islanding | Matched | 20 | 0 | 0 | 0 | 0 |
| Non-islanding | Switching of load | 1 | 9 | 0 | 0 | 0 |
| | Switching of Capacitor bank | 2 | 0 | 8 | 0 | 0 |
| | Faults | 0 | 0 | 0 | 10 | 0 |
| | Normal operation | 0 | 0 | 0 | 0 | 10 |
| Accuracy | | 95% | | | | |

Table 4.3: Performance matrix of DG1 (fold2).

| Fold (2) | | Islanding | Non-islanding | | | |
|---|---|---|---|---|---|---|
| | | Matched | Switching of load | Switching of Capacitor bank | Faults | Normal operation |
| Islanding | Matched | 20 | 0 | 0 | 0 | 0 |
| Non-islanding | Switching of load | 1 | 9 | 0 | 0 | 0 |
| | Switching of Capacitor bank | 0 | 0 | 10 | 0 | 0 |
| | Faults | 0 | 0 | 0 | 10 | 0 |
| | Normal operation | 0 | 0 | 0 | 0 | 10 |
| Accuracy | | 98.33% | | | | |

Table 4.4: Performance matrix of DG1 (fold3).

| Fold (3) | | Islanding | Non-islanding | | | |
|---|---|---|---|---|---|---|
| | | Matched | Switching of load | Switching of Capacitor bank | Faults | Normal operation |
| Islanding | Matched | 20 | 0 | 0 | 0 | 0 |
| Non-islanding | Switching of load | 1 | 9 | 0 | 0 | 0 |
| | Switching of Capacitor bank | 0 | 0 | 10 | 0 | 0 |
| | Faults | 0 | 0 | 0 | 10 | 0 |
| | Normal operation | 0 | 0 | 0 | 0 | 10 |
| Accuracy | | 98.33% | | | | |

Table 4.5: Performance matrix of DG2 (fold1).

| Fold (1) | | Islanding | Non-islanding | | | |
|---|---|---|---|---|---|---|
| | | Matched | Switching of load | Switching of Capacitor bank | Faults | Normal operation |
| Islanding | Matched | 20 | 0 | 0 | 0 | 0 |
| Non-islanding | Switching of load | 1 | 9 | 0 | 0 | 0 |
| | Switching of Capacitor bank | 2 | 0 | 8 | 0 | 0 |
| | Faults | 0 | 0 | 0 | 10 | 0 |
| | Normal operation | 0 | 0 | 0 | 0 | 10 |
| Accuracy | | 95% | | | | |

Table 4.6: Performance matrix of DG2 (fold2).

| Fold (2) | | Islanding | Non-islanding | | | |
|---|---|---|---|---|---|---|
| | | Matched | Switching of load | Switching of Capacitor bank | Faults | Normal operation |
| Islanding | Matched | 20 | 0 | 0 | 0 | 0 |
| Non-islanding | Switching of load | 0 | 10 | 0 | 0 | 0 |
| | Switching of Capacitor bank | 0 | 0 | 10 | 0 | 0 |
| | Faults | 0 | 0 | 0 | 10 | 0 |
| | Normal operation | 0 | 0 | 0 | 0 | 10 |
| Accuracy | | 100% | | | | |

Table 4.7: Performance matrix of DG2 (fold3).

| Fold (3) | | Islanding | Non-islanding | | | |
|---|---|---|---|---|---|---|
| | | Matched | Switching of load | Switching of Capacitor bank | Faults | Normal operation |
| Islanding | Matched | 20 | 0 | 0 | 0 | 0 |
| Non-islanding | Switching of load | 0 | 10 | 0 | 0 | 0 |
| | Switching of Capacitor bank | 1 | 0 | 9 | 0 | 0 |
| | Faults | 0 | 0 | 0 | 10 | 0 |
| | Normal operation | 0 | 0 | 0 | 0 | 10 |
| Accuracy | | 98.33% | | | | |

Table 4.8: Performance matrix of DG3 (fold1).

| Fold (1) | | Islanding | Non-islanding | | | |
|---|---|---|---|---|---|---|
| | | Matched | Switching of load | Switching of Capacitor bank | Faults | Normal operation |
| Islanding | Matched | 20 | 0 | 0 | 0 | 0 |
| Non-islanding | Switching of load | 0 | 10 | 0 | 0 | 0 |
| | Switching of Capacitor bank | 1 | 0 | 9 | 0 | 0 |
| | Faults | 0 | 0 | 0 | 10 | 0 |
| | Normal operation | 0 | 0 | 0 | 0 | 10 |
| Accuracy | | 98.33% | | | | |

Table 4.9: Performance matrix of DG3 (fold2).

| Fold (2) | | Islanding | Non-islanding | | | |
|---|---|---|---|---|---|---|
| | | Matched | Switching of load | Switching of Capacitor bank | Faults | Normal operation |
| Islanding | Matched | 20 | 0 | 0 | 0 | 0 |
| Non-islanding | Switching of load | 0 | 10 | 0 | 0 | 0 |
| | Switching of Capacitor bank | 0 | 0 | 10 | 0 | 0 |
| | Faults | 0 | 0 | 0 | 10 | 0 |
| | Normal operation | 0 | 0 | 0 | 0 | 10 |
| Accuracy | | 100% | | | | |

Table 4.10: Performance matrix of DG3 (fold3).

| Fold (3) | | Islanding | Non-islanding | | | |
|---|---|---|---|---|---|---|
| | | Matched | Switching of load | Switching of Capacitor bank | Faults | Normal operation |
| Islanding | Matched | 20 | 0 | 0 | 0 | 0 |
| Non-islanding | Switching of load | 2 | 8 | 0 | 0 | 0 |
| | Switching of Capacitor bank | 0 | 0 | 10 | 0 | 0 |
| | Faults | 0 | 0 | 0 | 10 | 0 |
| | Normal operation | 0 | 0 | 0 | 0 | 10 |
| Accuracy | | 96.67% | | | | |

The results for the three folds are summarized in Table 4.11:

Table 4.11: ANN performance for DG1, DG2 and DG3 for the 3 folds.

| Fold | DG1 | DG2 | DG3 |
|---|---|---|---|
| 1 | 95% | 95% | 98.33% |
| 2 | 98.33% | 100% | 100% |
| 3 | 98.33% | 98.33% | 96.67% |
| Average Accuracy | 97.22% | 97.77% | 98.33% |

## 4.5 Discussion

Results indicate that neuro-wavelet approach can detect islanding events with high degree of accuracy. The proposed method showed excellent performance for loads with high quality factor.

In this research, the WT analysis was carried on the voltage signal since the transients are clearer in the voltage signal than the current signal. In order to confirm this concept, the analysis was repeated and the current waveform was considered instead of the voltage. It is noticed from Tables 4.12- 4.14 that the voltage waveform results in better recognition rate than the current. Hence the voltage waveform is more discriminative than the current waveform. Additionally, the energies of the WT details for both the voltage and current waveforms were considered as feature vectors. However, the recognition rates did not change significantly compared to the rates obtained when considering the voltage waveform only. Thus, for less computational complexity voltage waveform only was considered in the analysis.

Table 4.12: ANN performance of DG1.

| **Fold** | **Training** | **Testing** | **Accuracy** | |
|---|---|---|---|---|
| | | | **Voltage** | **Current** |
| 1 | 120 | 60 | 95% | 81.67% |
| 2 | 120 | 60 | 98.33% | 80% |
| 3 | 120 | 60 | 98.33% | 81.67% |
| **Average accuracy** | | | 97.22% | 81.11% |
| **Average accuracy when voltage and current were used** | | | 97.22% | |

Table 4.13: ANN performance of DG2.

| Fold | Training | Testing | Accuracy | |
|---|---|---|---|---|
| | | | Voltage | Current |
| 1 | 120 | 60 | 95% | 81.67% |
| 2 | 120 | 60 | 100% | 95% |
| 3 | 120 | 60 | 98.33% | 81.67% |
| **Average accuracy** | | | 97.77 % | 86.11% |
| **Average accuracy when voltage and current were used** | | | 97.22% | |

Table 4.14: ANN performance of DG3.

| Fold | Training | Testing | Accuracy | |
|---|---|---|---|---|
| | | | Voltage | Current |
| 1 | 120 | 60 | 98.33% | 80% |
| 2 | 120 | 60 | 100% | 93.30% |
| 3 | 120 | 60 | 96.67% | 83.33% |
| **Average accuracy** | | | 98.33% | 85.55% |
| **Average accuracy when voltage and current were used** | | | 97.78% | |

Investigation of the Neuro-wavelet technique's response to addition of untrained DG is performed using the same system under study model. A fourth DG is added to the system model used before. The new DG is inverter based PV panel identical to the three old DGs. A total of 40 novel cases for the added DG4 are simulated and tested on the three ANN models for the three old DGs (DG1 ANN model, DG2 ANN model, and DG3 ANN model). The performance of ANN to an untrained DG is investigated and tabulated in Table 4.15.

Table 4.15: ANN performance of untrained DG4.

| **Model** | **Testing** | **Accuracy** |
|---|---|---|
| DG1 model | 60 | 93.33% |
| DG2 model | 60 | 98.33% |
| DG3 model | 60 | 98.33% |
| **Average accuracy** | | 96.66% |

It is evident from Table 4.15 that the ANN classifier was capable of differentiating between islanding and non-islanding events for the untrained fourth DG. Hence, there is no need to retrain the ANN model when adding a new identical DG. Also, training a common classifier when having identical DGs will result in high degree of accuracy instead of having separate model for each DG.

# CHAPTER 5

# CONCLUSIONS AND RECOMMENDATIONDS

Many schemes have been proposed to detect islanding such as passive, active and communication based techniques. Passive techniques work well when there is power imbalance between the power generated from the DG and the power consumed form the load. On the other hand, active methods affect the power quality and do not perform well in the presence of multiple DGs. Though communication based islanding detection techniques have no NDZ techniques, they are costly and complex.

The performance of two commonly used passive anti-islanding techniques was validated by computer simulation. These techniques are under/over frequency (UOF), under/over voltage (UOV), and detection of harmonics (DH) passive anti-islanding schemes. UOV/UOF passive technique work well when there is a power imbalance between the power generated from the DG and the power consumed from the load. However, these methods fail to detect islanding under power balanced conditions. Based on the specified interface, it was verified that UOF/UOV techniques have large NDZ. On the contrary, in the DH method it is difficult to select an appropriate threshold that provide islanding detection but do not lead to false tripping. These techniques are not capable of detecting islanding alone and should be combined with other techniques especially in the presence of multiple DGs in the distribution network.

The neuro-wavelet based islanding technique was successfully implemented for multiple three phase inverter interfaced DGs. Wavelet transform is capable of decomposing the voltage signals into different frequency bands. It can be utilized in extracting discriminative features from the acquired voltage signals. The energy

content of wavelet details are then calculated and fed to a trained ANN which is capable to differentiating between islanding and non-islanding events.

Implementing neuro-wavelet based anti-islanding technique using the feature vectors extracted from the voltage signals yields superior performance in terms of the detection rate than that extracted from the current signals. However, considering the features extracted from both the voltage and current signals resulted in insignificant change of the detection rates compared to the rates obtained when considering the voltage waveforms only. Thus, for less computational complexity voltage waveforms were only considered in the analysis. Analysis of the response of the proposed method to addition of identical untrained DG was examined. Simulation results verified that the islanding cases were successfully detected in case of adding untrained identical DGs since the voltage transients generated is identical. Hence using a common trained model for all the identical connected DG is capable of detecting the islanding event rather than training separate models for each DG in the island.

The simulation results proved that the proposed method is immune to any changes of the connected load. The method has good performance for parallel RLC loads having quality factor of 2.5. Normally the load connected on the distribution feeder has a quality factor of 2.5 or less. Moreover, since the proposed method is categorized under passive techniques it has no negative effect on the power quality.

## 5.1 Future work

Though the proposed method resulted in very good accuracy rate, the technique has been validated using relatively small testing set. Increasing the testing data set will result in more general and accurate recognition rate. The proposed technique was implemented on one system configuration. To increase confidence in these results, similar simulations could be performed using different system models. Another direction for future work is to implement and verify the proposed approach with practical and real time implementation.

# REFERENCES


[1] E. F. El-Saadany, H. H. Zeineldin, and A. H. Al-Badi, "Distributed generation: benefits and challenges," in International Conference on Communication, Computer & Power, 2007, pp. 115-119.

[2] A. Algarni, "Operational and planning aspects of distribution systems in deregulated electricity markets," Ph.D. dissertation, University of Waterloo, Waterloo, ON, Canada 2009.

[3] H.H. ZeinElDin, E.F. El-Saadany, and M.M.A. Salama, "Islanding Detection of Inverter Based Distributed Generation," in IEE Proceedings in Generation, Transmission and Distribution, Vol. 153, No. 6, Nov. 2006, pp. 644 – 652.

[4] M. A. Eltawil, Z. Zhao, "Grid-connected photovoltaic power systems: Technical and potential problems—A review" Renewable and Sustainable Energy Reviews, Vol. 14, 2009, pp. 112–129.

[5] United States of America. Congress of the U.S., Congressional Budget Office. Prospects for distributed electricity generation. September, 2003.

[6] J. K. Tailor and A.H. Osman, "Restoration of Fuse-Recloser Coordination in Distribution System with high DG Penetration," in IEEE Power and Energy Society General Meeting, Jun. 2008, pp. 1 – 8.

[7] W. Xu, K. Mauch, S. Martel "An assessment of distributed generation islanding detection methods and issues for Canada" CANMET energy technology center, 2004.

[8] V. Menon and M. H. Nehrir, "A Hybrid Islanding Detection Technique Using Voltage Unbalance and Frequency Set Point" in IEEE Transaction on power systems, Vol. 22, No. 1, Feb. 2007, pp. 442-448.

[9] N. W. A. Lidula, N. Perera, "Investigation of a Fast Islanding Detection Methodology Using Transient Signals," Natural Sciences and Engineering Research Council (NSERC) of Canada, 2009.

[10] K. El-Arroudi, G. Joós, I. Kamwa, and D. T. McGillis, "Intelligent-Based Approach to Islanding Detection in Distributed Generation" in IEEE Transaction On power Del., Vol. 22, No. 2, Apr. 2007, pp. 828-835.

[11] M. Bayrak “Recurrent artificial neural network based islanding protection by using generator speed deviation” Scientific Research and Essay Vol.4, Apr. 2009, pp. 212-216,

[12] W. Bower, M. Ropp “Evaluation of islanding detection methods for photovoltaic utility-interactive power systems” in International Energy Agency, Mar. 2002.

[13] W. Freitas, W. Xu, C. M. Affonso, Z. Huang “Comparative Analysis Between ROCOF and Vector Surge Relays for Distributed Generation Application,” in IEEE Transaction Power Del., Vol. 20, No. 2, Apr. 2005, pp. 1315-1324.

[14] S. K. Salman, D. J. King, G. Weller, “New loss of mains detection algorithm for embedded generation using rate o change of voltage and changes in power factors,” in Seventh International Conference on (IEE) Developments in Power System Protection, Apr. 2001, pp. 82-85.

[15] M. B. Reynen, A. H. Osman and O. P. Malik “Using gold sequences to improve the performance of correlation based islanding detection” in Electric Power Systems Research, Vol. 80, No. 6, Jun. 2010, pp. 733-738.

[16] B. Bahrani, H. Karimi, and R. Iravani “Nondetection Zone Assessment of an Active Islanding Detection Method and its Experimental Evaluation,” In IEEE Transaction on Power Del, Vol.99, 2009, pp. 1-9.

[17] J. Yin, L. Chang, and C. Diduch, “A new hybrid anti-islanding algorithm in grid connected three-phase inverter system,” in IEEE Power Electronics Specialist Conference (PESC’06), Jun. 2006, pp. 1-7.

[18] W. Xu, G. Zhang, C. Li, W. Wang “A Power Line Signaling Based Technique for Anti-Islanding Protection of Distributed Generators—Part I: Scheme and Analysis,” In IEEE Transaction on Power Del. Vol. 22, No. 3, Jul. 2007, pp. 1758 – 1766.

[19] R. Kunte “A wavelet transform-based islanding detection algorithm for inverter assisted distributed generators” Ms.c. thesis, Tennessee Technological University, 2009.

[20] A. Pigazo, M. Liserre, R. Mastromauro,V. Moreno, A. Dell'Aquila “ Wavelet-Based Islanding Detection in Grid-Connected PV Systems,” In IEEE transaction on Ind. Electron., Vol. 56, No. 11, Nov. 2009, pp. 4445-4455.

[21] Z. Ye, A. Kolwalkar, Y. Zhang, P. Du and Reigh Walling “Evaluation of anti-islanding schemes based on nondetection zone concept” in IEEE transactions on power electronics, Vol. 19, No. 5, Sep. 2004, pp. 1171 - 1176

[22] X. Wang, W. Freitas, W. Xu, and V. Dinavahi, “Impact of interface controls on the steady state stability of inverter based distributed generators,” in Power Engineering Society General Meeting, Jun. 2007, pp. 1–4.

[23] M. Tarafdar Haque, and A.M. Kashtiban,” Application of Neural Networks in Power Systems; A Review” World Academy of Science, Engineering and Technology 6, 2005.

[24] Hagan, M.T., H.B. Demuth, and M.H. Beale, *Neural Network Design*,Boston, MA: PWS Publishing, 1996.

[25] C. Parameswariah, and M. Cox “Frequency Characteristics of Wavelets,” In IEEE Power Engineering Review, Vol. 22, Jan. 2002.

[26] S.Chen, “Feature selection for identification and classification of power quality disturbances,” Power Engineering Society General Meeting, 2005. IEEE, Vol. 3, pp. 2301-2306.

[27] A. H. Osman, O. P. Malik “Transmission Line Distance Protection Based on Wavelet Transform,” In IEEE transaction on Power Del., Vol. 19, No. 2, Apr. 2004, pp. 515-523.

[28] D. T. K. Viet, K. Agbossou, and M. L. Doumbia, “Islanding detection for utility interconnection of multiple distributed generators,” in Canadian Conference on Electrical and Computer Engineering, May 2008, pp. 557–560.

[29] O. Tsukamoto and K. Yamagishi, “Detection of islanding of multiple dispersed photovoltaic power systems,” Solar Energy, vol. 58, no. 1-3, pp. 9–15, 1996.

# APPENDIX A

The PSCAD simulation model is shown in the figure below:

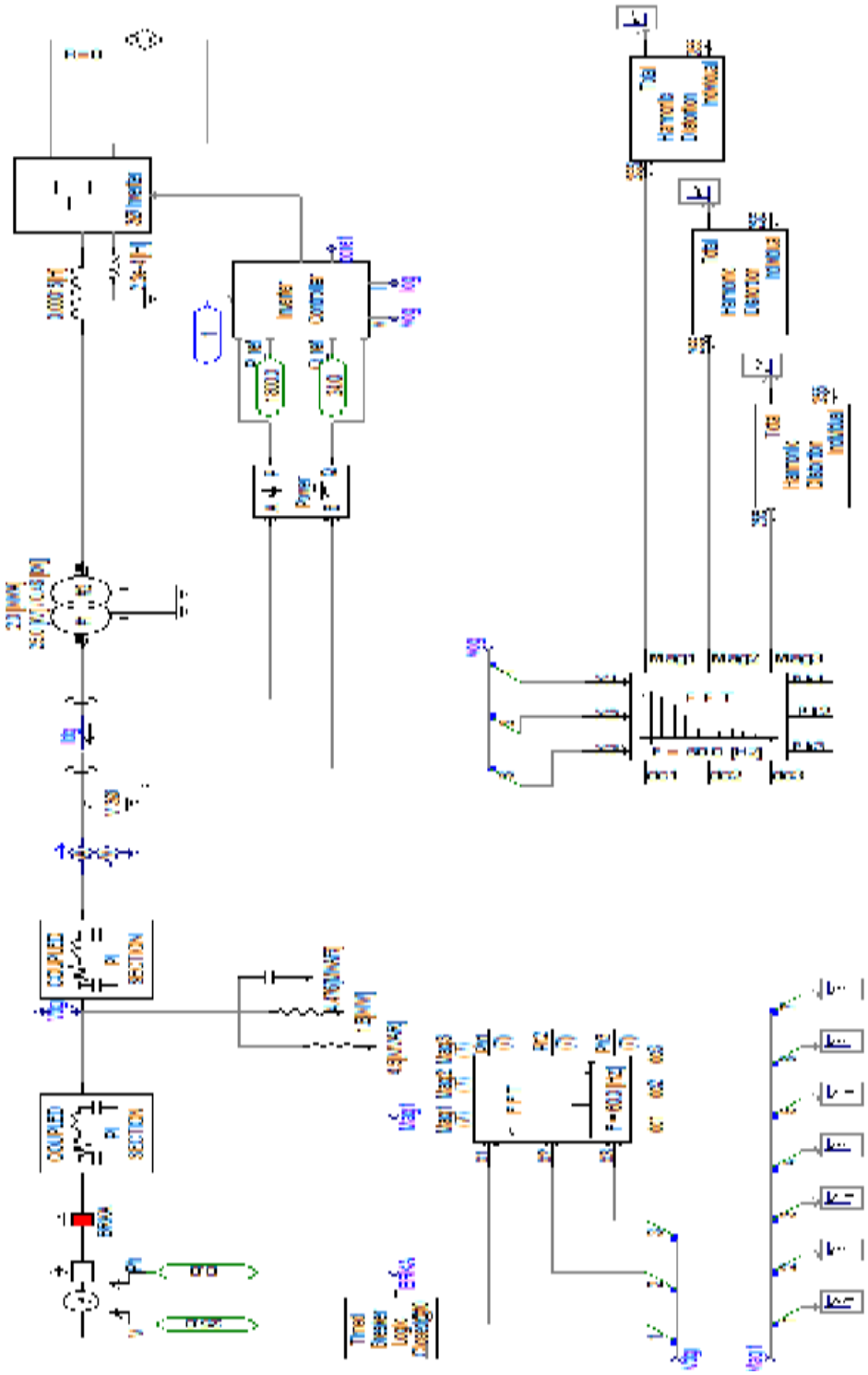

Figure A. 1: PSCAD simulation of the system model

The inverter's controller is shown in the figure below

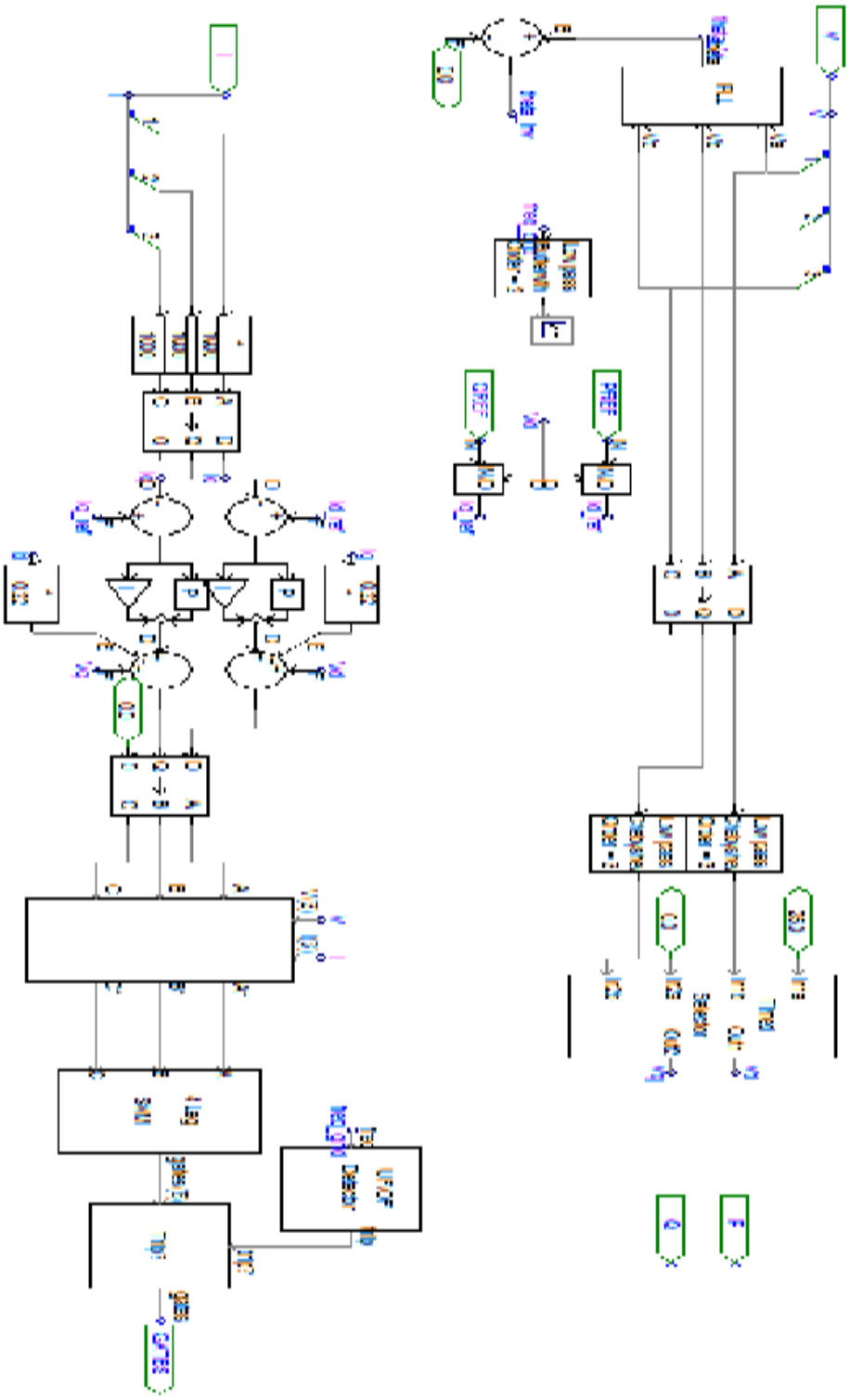

Figure A.2: the inverter controller

The inverter's controller is shown in the figure below

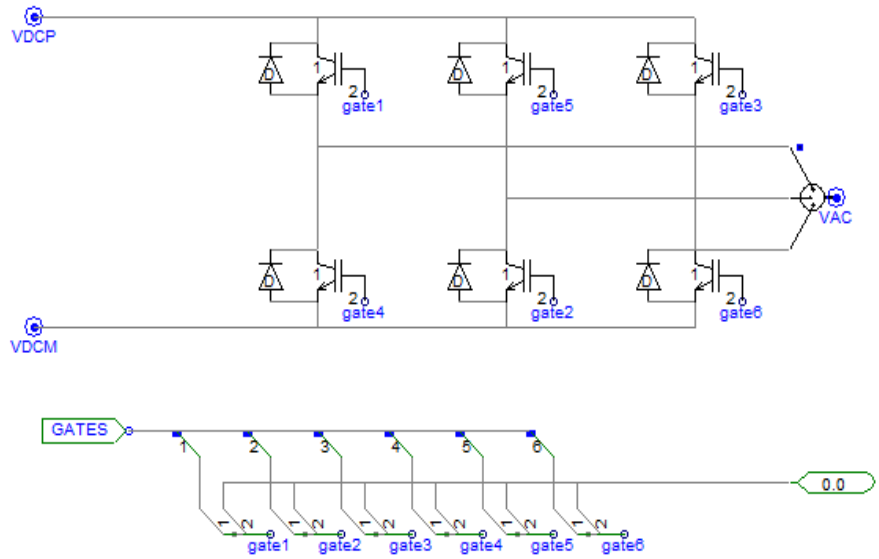


Figure A. 3: Three leg inverter inverter

# APPENDIX B

Derivation of U/OF and U/OV NDZ is found in [21]

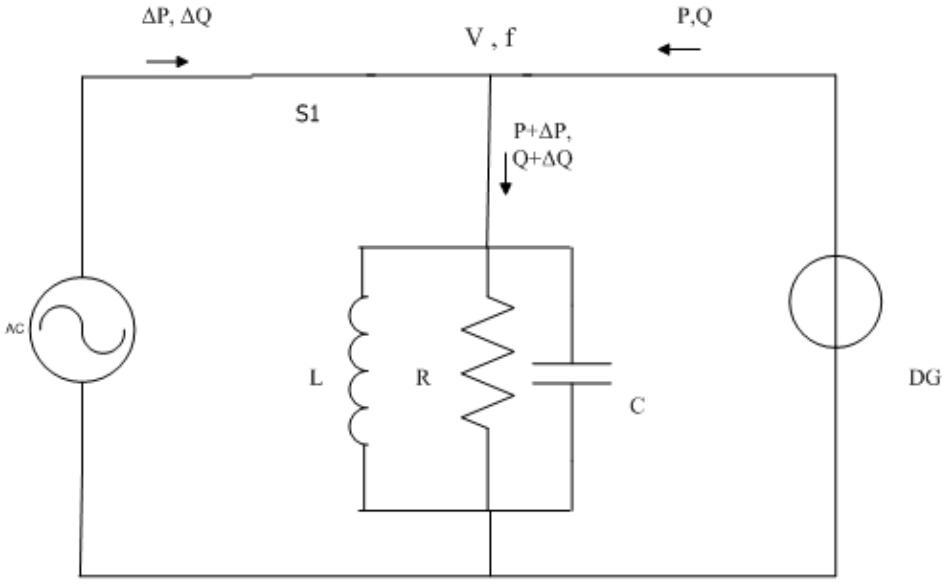


Figure B.1: generic system for anti-islanding study

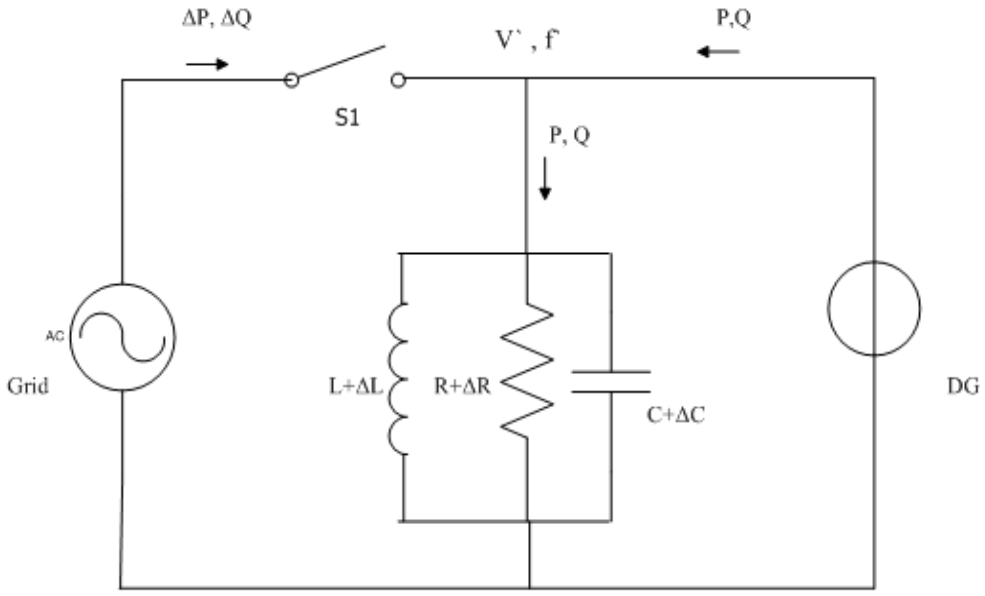


Figure B.2: DG and RLC load after islanding

In Figure A.2, an island is formed and the DG.

The new load resonant frequency is

$$f' = \frac{1}{2\pi\sqrt{(L+\Delta L)\times(C+\Delta C)}} \tag{B.1}$$

The following equation can be obtained:

$$\frac{f'-f}{f} = \frac{\frac{1}{2\pi\sqrt{(L+\Delta L)\times(C+\Delta C)}} - \frac{1}{2\pi\sqrt{(L\times C)}}}{\frac{1}{2\pi\sqrt{(L\times C)}}} \tag{B.2}$$

$$= \frac{\sqrt{L\times C}}{\sqrt{(L+\Delta L)\times(C+\Delta C)}} - 1 \tag{B.3}$$

Given the frequency thresholds $f_{min}$, and $f_{max}$, in order for $f'$ to be within the thresholds, the following condition must be met:

$$\frac{f_{min}-f}{f} \leq \frac{\sqrt{L\times C}}{\sqrt{(L+\Delta L)\times(C+\Delta C)}} - 1 \leq \frac{f_{max}-f}{f} \tag{B.4}$$

This expression can be simplified with approximation of $\Delta L \times \Delta C \approx 0$;

$$\left(\frac{f}{f_{max}}\right)^2 - 1 \leq \frac{\Delta L}{L} + \frac{\Delta C}{C} \leq \left(\frac{f}{f_{min}}\right)^2 - 1 \tag{B.5}$$

The relationship between $\Delta L$ and $\Delta C$ can be derived as

$$\Delta Q = V^2 \times \left(\frac{1}{2\pi\times f\times(L+\Delta L)} - 2\pi\times f\times(C+\Delta C)\right) \tag{B.6}$$

$$= V^2 \times \left(\frac{1}{2\pi\times f\times L\left(\frac{1+\Delta L}{L}\right)} - 2\pi\times f\times C\left(\frac{1+\Delta C}{C}\right)\right) \tag{B.7}$$

$$= \frac{Q_L}{\frac{1+\Delta L}{L}} - Q_C \times \left(\frac{1+\Delta C}{C}\right) \quad (B.8)$$

Based on $Q_f$ definition, there is

$$Q_L = Q_C = Q_f \times P \quad (B.9)$$

Then the normalized $\Delta Q$

$$\frac{\Delta Q}{P} = \frac{Q_f}{\frac{1+\Delta L}{L}} - Q_f \times \left(\frac{1+\Delta C}{C}\right) \quad (B.10)$$

$$= Q_f \times \frac{1 - \left(\frac{1+\Delta L}{L}\right) \times \left(\frac{1+\Delta C}{C}\right)}{\frac{1+\Delta L}{L}} \quad (B.11)$$

$$\approx Q_f \times \frac{\frac{-\Delta L}{L} - \frac{\Delta C}{C}}{\frac{1+\Delta L}{L}} \approx -Q_f \times \left(\frac{\Delta L}{L} + \frac{\Delta C}{C}\right) \quad (B.12)$$

Here, two approximations are made

1. $\Delta L \times \Delta C \approx 0$;
2. $1 + \frac{\Delta L}{L} \approx 1$.

From A.5 and A.12, the following equation is obtained

$$Q_f.\left(1 - \left(\frac{f}{f_{min}}\right)^2\right) \leq \frac{\Delta Q}{P} \leq Q_f.\left(1 - \left(\frac{f}{f_{max}}\right)^2\right) \quad (B.13)$$

Similarly, the relationship between the voltage and active power is derived as follows:

Before islanding the load active power is $\frac{V^2}{R}$ after islanding the active power is $\frac{V^2}{R+\Delta R}$. Assuming the DG is constant power control, and then the balance of active power gives:

$$\frac{V'^2}{R+\Delta R} = \frac{(V+\Delta V)^2}{R+\Delta R} = \frac{V^2}{R} \qquad (B.14)$$

Equation A. 14 can be simplified as

$$\frac{\Delta R}{R} = 2\frac{\Delta V}{V} + \left(\frac{\Delta V}{V}\right)^2 \qquad (B.15)$$

Before islanding the grid supplies $\Delta P$ to the RLC load

$$\Delta P = \frac{V^2}{R+\Delta R} - \frac{V^2}{R} \qquad (B.16)$$

Normalize $\Delta P$

$$\frac{\Delta P}{P} = \frac{\frac{V^2}{R+\Delta R} - \frac{V^2}{R}}{\frac{V^2}{R}} = \frac{\Delta R}{\Delta R + R} = -\frac{\frac{\Delta R}{R}}{\frac{\Delta R}{R+1}} \qquad (B.17)$$

Substituting (A.15) into (A.17) and simplifying the equation, the following equation will be obtained:

$$\frac{\Delta P}{P} = -\frac{2\frac{\Delta V}{V} + \left(\frac{\Delta V}{V}\right)^2}{2\frac{\Delta V}{V} + \left(\frac{\Delta V}{V}\right)^2 + 1} = \frac{1}{\left(\frac{\Delta V}{V}+1\right)^2} - 1 \qquad (B.18)$$

Given the voltage thresholds, $V_{max}$ and $V_{min,}$ and in order for V` to be within the thresholds, the following condition should be met.

$$\left(\frac{V}{V_{max}}\right)^2 - 1 \le \frac{\Delta P}{P} \le \left(\frac{V}{V_{min}}\right)^2 - 1 \qquad (B.19)$$

# VITA

Yara Walid Fayyad was born on June 5, 1987, in Nablus, Palestine. She was educated in local public schools in Qatar. She graduated from high School holding the sixth rank among Qatar government's school in 2004. She received her Bachelor's degree with cam laude in Electrical Engineering from the American university of Sharjah in 2008. In 2008, Ms. Fayyad was awarded a scholarship from the American University of Sharjah to continue her master's degree in Electrical Engineering. She was awarded the Master of Science degree in electrical engineering program in 2010.